To the Graduate Council:

I am submitting herewith a thesis written by Derek Keith Gowanlock entitled "Experimental Study of the Control of Rotor Tip Vortices Using Discrete Blade Tip Jets". I have examined the final copy of this thesis for form and content and recommend that it be accepted in partial fulfillment of the requirements for the degree of Master of Science, with a major in Aerospace Engineering.

A.D. Vakili, Major Professor

We have read this thesis and
Recommend its acceptance:

Accepted for the council:

Associate Vice Chancellor and
Dean of the Graduate School

EXPERIMENTAL STUDY OF THE CONTROL OF ROTOR TIP VORTICES USING DISCRETE BLADE TIP JETS

A Thesis Presented for the

Master of Science

Degree

The University of Tennessee, Knoxville

Derek Keith Gowanlock

August 1998

ACKNOWLEDGEMENTS

I gratefully acknowledge the love and support always provided by my family. I especially thank my wife Jennifer whose love and friendship gave me the strength and motivation to achieve and my parents Bruce and Eunice Gowanlock who have supported and guided me in every endeavor I have undertaken. I also thank my brother David, whose competitive motivation and friendship have always been an encouraging factor in my life. (I guess you have to go to graduate school now.)

I must also pay tribute to the entire UTSI staff, whose support and guidance have been instrumental in my postgraduate success. In particular I would like to thank my advisor Dr. Vakili, whose insight and drive were fundamental to the success of both this project and my post graduate career, in general. As well, I would like to thank Ricky Meeker whose support day in and day out was indispensable. The special efforts contributed by Dr. Merkle and Dr. J.Z. Wu as committee members for my thesis are also greatly appreciated.

Per Ardua Ad Astra

ABSTRACT

An experimental study of the effects of destabilizing rotor tip vortices using perturbations introduced by discrete tip jets has been carried out. Both flow visualization and Particle Image Velocimetry (PIV) were conducted on a rotor test stand to evaluate the effectiveness of discrete jets on a rotary wing application, with the aspiration of reducing the effects of blade vortex interaction – a common problem in rotor aeroacoustics. Flow visualization tests of the rotor wake flow field ($Re \cong 300\,000$) revealed a relative outward radial movement of the vortex core in the vicinity of the rotor tip, for the case with tip blowing ($C\mu = 0.0774$). Visualization also indicated a reduction in the coherence of the vortices shed from the modified blade. PIV testing revealed a significant dispersion of velocity and vorticity in both the near field and far field of the rotor wake flow ($Re \cong 300\,000$) with blowing at approximately $C\mu = 0.02$. In the near field, vortex core displacement was verified for the one-blade-blowing configuration. As well significant dispersion of the vortex velocity field was observed. In the far field (2 ½ revolutions downstream) no distinct vortex was visible when blowing was issued from both blades as compared to only minor diffusive changes for the baseline (no blowing) configuration at that location. The results obtained qualitatively and quantitatively indicate the potential benefits of discrete tip jets as a means of rotor tip wake control.

TABLE OF CONTENTS

CHAPTER		PAGE
I.	INTRODUCTION	1
II.	BACKGROUND AND THEORETICAL CONSIDERATIONS	3
	Literature Review and Background Considerations	3
III.	FLOW VISUALIZATION AND PIV TESTS	17
	Experimental Objectives	17
	General Experimental Set-Up	17
	Flow Visualization Test Set-Up	20
	Flow Visualization Test Conditions	22
	PIV Test Set-Up	22
	PIV Test Conditions	27
IV.	RESULTS AND DISCUSSION	29
	Flow Visualization Results and Discussion	29
	PIV Test Data – Post Processing	32
	PIV Test Results and Discussion	38
V.	CONCLUSIONS AND RECOMMENDATIONS	52
LIST OF REFERENCES		54
VITA		58

LIST OF FIGURES

FIGURE		PAGE
2-1	Vortex Sheet Trailing Behind a Wing	5
2-2	Helmholtz Vortex Law's Interpretation of Tip Vortices	6
2-3	Generalized Flow Field Schematic for a Hovering Helicopter	7
2-4	Typical Flow Phenomenon Found on a Helicopter in Forward Flight	8
2-5	Persistent Wingtip Vortex Due to a Lifting Surface – Water Tunnel Dye Injection Flow Visualization	12
2-6	Wingtip Vortex Dispersed by Wingtip Flow Control – Water Tunnel Dye Injection Flow Visualization	12
2-7	Vortex Effective Velocity vs. Time - Baseline	13
2-8	Vortex Effective Velocity vs. Time – 1 Blade Blowing	13
3-1	Rotor Test Stand Schematic	18
3-2	Rotor Hub Assembly	19
3-3	Modified Rotor Blade Tip	19
3-4	Schematic of NACA 0012-64 Model Rotor Blade	20
3-5	Flow Visualization Set-Up	21
3-6	Lab Set-Up for PIV Tests	24
3-7	Smoke Particle Generation and Insertion Apparatus	26
4-1	Smoke Flow Visualization (No Blowing)	30
4-2	Smoke Flow Visualization (1 Blade Blowing)	30
4-3	Vortex Merging (No Blowing)	31
4-4	PIV Test Data Post-Processing Example of Raw Data	34
4-5	PIV Test Data Post-Processing Example of Raw Data with Range Filter Applied	35
4-6	PIV Test Data Post-Processing Example of Raw Data with Range Filter and Median Filter Applied	36

4-7 PIV Test Data Post-Processing Example of Raw Data with Range Filter, Median Filter and Gaussian Smoothing Applied 37
4-8 PIV Results – No Blowing, Near Field Velocity Contour 42
4-9 PIV Results – No Blowing, Near Field Vorticity Contour 43
4-10 PIV Results – 1 Blade Blowing, Near Field Velocity Contour 44
4-11 PIV Results – 1 Blade Blowing, Near Field Vorticity Contour 45
4-12 PIV Results – No Blowing, Near Field, Wide View Velocity Contour 46
4-13 PIV Results – 2 Blades Blowing, Near Field, Wide View Velocity Contour 47
4-14 PIV Results – No Blowing, Far Field Velocity Contour 48
4-15 PIV Results – 2 Blades Blowing, Far Field Velocity Contour 49

LIST OF SYMBOLS

A_j	Area of the jet port
b	Wing (blade) span
BVI	Blade Vortex Interaction
c	Wing (blade) chord
Cμ	Jet blowing (momentum) coefficient $C\mu=2\dot{m}_j \cdot V_j/(\rho \cdot V_{tip}^2 \cdot S)$,
d_s	Jet slot width
f_j	Jet frequency (cycles per second)
L_s	Jet slot length
$\dot{m}_j$	Jet mass flow rate
N	Rotor angular velocity
P_j	Jet pressure
PIV	Particle Image Velocimetry
Re	Reynolds Number
RPM	Revolutions per minute
S	Planform area of wing (rotor blade)
TSI	Thermal Systems Incorporated
U	X-component of velocity
UTSI	University of Tennessee Space Institute
V	Y-component of velocity
V_j	Jet velocity
V_{tip}	Rotor tip velocity
α	Angle of Attack
δ_c	Distance between jet ports along the chord line
δ_v	Vertical distance of jet slot centre line above/below the chord line
Θ_{di}	Dihedral angle of injected jet
Θ_{sweep}	Sweep angle of injected jet
ρ_a	Density of ambient air

ρ_j	Density of jet
μ	Ambient and jet fluid viscosity
ω	Vorticity (cycles per second)

Chapter 1

INTRODUCTION

Since d'Alembert's realization that an arbitrary body in an ideal flow has no resultant force applied to it, fluid and aerodynamicists have studied the resistive force known as drag. In almost all cases this investigation has been directed at attempts to reduce the body's inherent drag for a specific flow. In real three-dimensional flows, for example, it is known that the drag experienced by the body in the flow can be divided into several parts. Specifically, drag can be broken down into two major contributory components: profile drag (composed of form and skin friction drag) and induced drag (drag due to lift and the associated three dimensional effects). As a result of this knowledge, many hours of experimentation and theoretical analysis have been spent on trying to improve or decrease the contribution of each of these components. As this research was conducted into the forms of drag and their contributory structures, the critical roll of wingtip vortices in the formation of induced drag was revealed.

Wingtip vortices are an undesirable by-product of the generation of lift by a three-dimensional body. However, their influence goes far beyond that of aerodynamic inefficiency. In the aviation industry, the interactions between wingtip vortices and other aircraft and aircraft structures are well known. Not only do concerns of aircraft-vortex interactions cause delays between aircraft departing or arriving at an airport but they also have been the cause of several serious aircraft accidents. The vortices generated from a helicopter rotor blade tip provide even more complications as the vortex shed from a particular blade interact with other rotor blades and the helicopter structure itself.

These vortex related problems have formed the impetus for the vast amounts of investigation that has been spent in the field of tip vortex attenuation and control. Despite all the research conducted into minimizing tip vortices, the nature of vortex stability and breakdown is not fully understood and an accurate theoretical model to

predict vortex stability still remains to be defined. This study is an experimental investigation into the effects of small, steady, spatially discrete jets of air, issued from a rotor tip, on the tip vortices shed from a model helicopter rotor. Initially basic flow visualization was carried out to help better visualize and understand the results achieved in previous investigations. Then, using Particle Image Velocimetry (PIV) the flow's velocity field was quantified for several comparative cases. The following Chapters will present some of the related background information (Chapter II), the experimental objectives and test set-up (Chapter III) and will conclude with a discussion of the results (Chapter IV) and conclusions (Chapter V).

Chapter II

BACKGROUND AND THEORETICAL CONSIDERATIONS

Literature Review and Background Considerations

The study of tip vortex control is not a new area of research. In fact for more than fifty years researchers have been examining ways to control and/or minimize tip vortices. This chapter serves to summarize those pertinent findings from the extensive field of work involving wingtip vortices. First, the basic physics of wingtip vortices will be discussed. Next, the motivating factors behind this specific investigation will be presented. Finally, a discussion of the work that has led to this specific avenue of tip vortex research will be detailed.

Vorticity – A Brief Review

The vorticity, $\vec{\omega}$, of a flow field with velocity distribution $\vec{u}$, is defined by $\vec{\omega} = \nabla \times \vec{u}$ and has the dimensions of a frequency (i.e. s^{-1}). In simple terms, vorticity is a measure of a fluid element's rotation about its own axis. A vortex can be defined as "a compact region of vorticity, possibly unbounded in one direction, surrounded by irrotational fluid. Strictly speaking the viscosity has to vanish for this definition to make sense, but (it is supposed) that the viscosity is very small and (therefore) allow transcendentally small vorticity outside the vortex."[1] A property that is closely related to vorticity is the fluid circulation, Γ, and is defined for any closed curve, C, in a fluid as $\Gamma = \oint_C \vec{u} \cdot d\vec{l}$. The relationship between vorticity and circulation can be mathematically expressed as $\Gamma = \int_S \vec{\omega} \cdot \vec{n} dS$, where S is any surface bounded by curve C. Basically, the circulation around a closed curve equals the net vorticity flux through the enclosed surface.

Kelvin and Helmholtz have developed theorems governing the conservation of vorticity and circulation in ideal flows. They have shown that for a two dimensional, inviscid flow vorticity is transported with fluid particles. For homogeneous, incompressible and viscous fluids under the influence of conservative body forces, vorticity is generated only through solid boundaries. For such a fluid flow, vorticity changes from one point to another by convection, vortex stretching/tilting, by diffusion due to viscosity and/or viscous dissipation. As one moves with a fluid element its vorticity changes are governing by the vorticity transport equation:

$$\frac{D\vec{\omega}}{Dt} = \vec{\omega} \cdot \nabla \vec{u} + \nu \nabla^2 \vec{\omega}$$

This equation is analogous to the momentum equation for velocity and describes how vorticity changes (in the material sense) with stretching/tilting and diffusion.

There is also an equation which parallels the kinetic energy equation (for velocity) and is expressed in terms of enstrophy, ω^2 (a scalar measure of vorticity magnitude):

$$\frac{D\left(\frac{1}{2}\omega^2\right)}{Dt} = \vec{\omega} \cdot \nabla \vec{u} \cdot \vec{\omega} + \nu \nabla^2 \left(\frac{1}{2}\omega^2\right) - \nu(\nabla \vec{\omega} : \nabla \vec{\omega})$$

This equation can be derived by simply taking the inner product of the vorticity transport equation and vorticity ($\vec{\omega}$). The significance of this second equation is found in the last term, which shows that for any existing vorticity gradient, there will always be a decrease (dissipation) in the total vorticity. Therefore, the only mechanism for a net change in the strength of a vortex tube is through viscous diffusion and dissipation. If the fluid viscosity is very low, as is the case for air, then the diffusion and dissipation is weak. The rate of viscous diffusion increases as local velocity gradients increase and as flow uniformity is decreased. Similarly, dissipation increases with increased local vorticity gradients.

The presence of a vortex, specifically a wingtip vortex, in a flow can be theoretically explained many different ways. Prandtl's Model[2] for flow past a finite wing provides one explanation of wingtip vortex formation. According to Prandtl's Model,

associated with the lift on a wing there is circulation around the wing (the Circulation Theory of Lift). Since the lift generated by the wing varies along its span, so must the circulation vary. From the definition of circulation it is known that the circulation around any wing section must be equal to the outflow of vorticity through that section. Therefore, the variation of lift and circulation along the span of a wing is accompanied by the shedding of vorticity from the wing. If the circulation varies continuously along the wing span, a continuous sheet of vorticity (predominately oriented with the mean flow) proceeds from the wing. This sheet is known as a trailing vortex sheet. If the circulation (and lift) are zero at the wingtips, a concentrated vorticity filament (i.e. a vortex) will be shed from each wingtip (Figure 2-1).

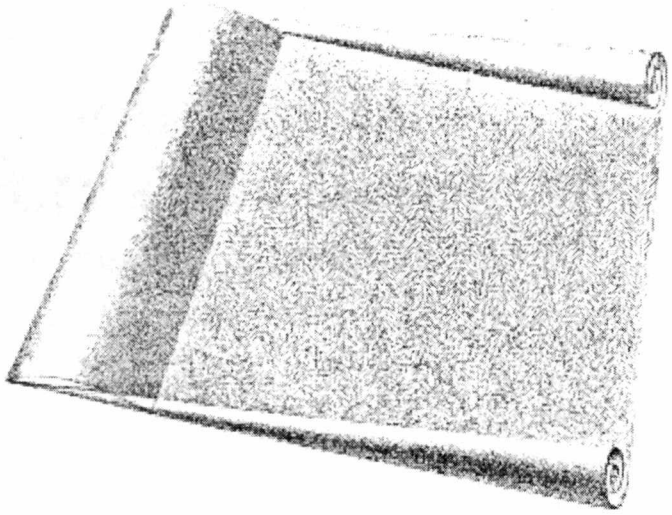


Figure 2-1. Vortex Sheet Trailing Behind a Wing[2]

Similarly, for a finite length wing impulsively started from rest, the Kutta-Joukowski Theorem[3] requires that there must exist a net circulation around the wing for lift to be able to be generated (creating a "bound" vortex). However, since Kelvin's Theorem (for inviscid, incompressible flows) requires that the net circulation be constant at any time, an equal and opposite amount of circulation (called the "starting" vortex) must be shed when the wing starts moving. Since vortex lines cannot end in a fluid, these two vortices must be connected, by tip vortices, as illustrated in Figure 2-2.

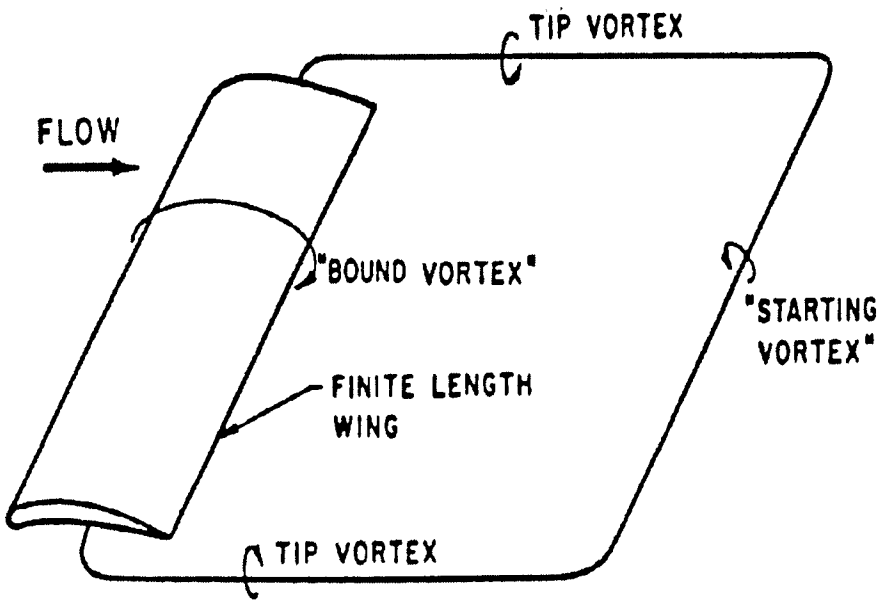


Figure 2-2. Helmholtz Vortex Laws Interpretation of Tip Vortices[3]

Wingtip vortices can also be explained physically. A wing that is moving through a fluid and generating net lifting forces (i.e. aerodynamic lift) will, obviously, be exposed to differential pressures. Naturally, at the wingtip, the flow will be accelerated from the high-pressure side of the wing to the low-pressure side of the wing. This motion of the fluid at the wingtip, combined with the net flow creates a helical flow extending from the wingtip – a wingtip vortex. Figure 2-5 shows a classic fixed wingtip vortex, as visualized in a water tunnel experiment.

Wingtip vortices are likewise generated on the blades of a helicopter. However, in the helicopter application, the blade rotation and axial flow causes the blade tip vortices to form in a helical pattern as illustrated in Figure 2-3. This vortex shedding geometry is further complicated by many factors including the direction of flight, airframe structure and rotor aerodynamics, all which have the effect of deforming the helical vortex structure.

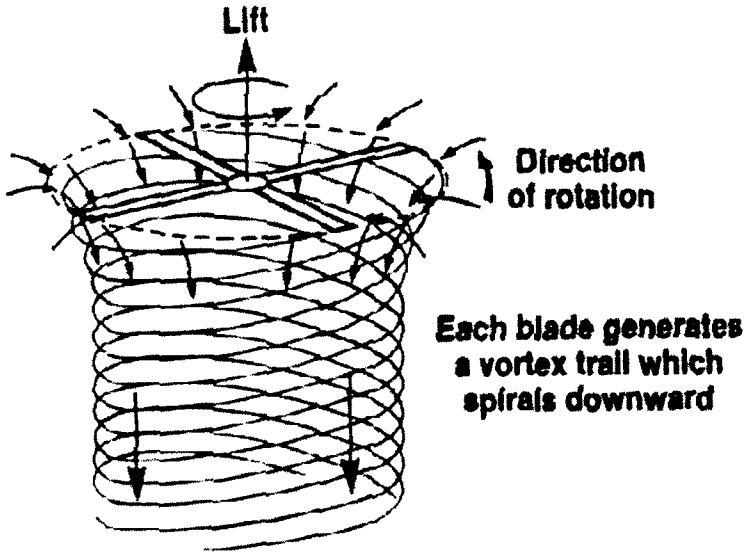


Figure 2-3. Generalized Flow Field Schematic for a Hovering Helicopter[4]

Motivations and Methods to Minimize the Tip Vortex

The generation of vorticity due to a lifting surface in a fluid is inevitable. Nonetheless, there can be great advantage if the concentrations of this vorticity can be controlled. For a three-dimensional wing, the trailing vortex system imparts a downwash on the wing (which is strongest at the location of highest vorticity – at the wingtip). This downwash effectively tilts back the lift vector or decreases the local angle of attack and thus transfers some of the lift into drag. This effect is known as induced drag and is a purely three-dimensional effect. Wingtip vortices can be the cause of other problems as well. Several well-documented flight accidents have occurred when small aircraft have lost control authority after flying into a vortex shed by larger aircraft. This is an effect related to the total circulation of the vortex that is shed by the larger aircraft. In the application of a helicopter rotor, the vortices shed from the rotor can interact with other rotor vortices, the airframe, the tail rotor and with other main rotor blades (called Blade-Vortex Interaction – BVI)[5,6]. Examples of these phenomena are illustrated in Figure 2-4. BVI, in particular, can produce very high blade loads and can generate impulsive noise and structural vibration. Although the derivation is beyond the scope of this

investigation, it should be noted that the impulsive noise generated from a structure-vortex interaction is a function of the pressure gradient of the flow field. Of course, the pressure gradient is also a function of the flow field velocity gradient. It is precisely these adverse consequences of the existence of tip vortices that vortex attenuation (in the form of an increased rate of vortex dispersion) could minimize, while providing an improvement in the aerodynamic efficiency of the wing or blade. It is for these reasons that this investigation was undertaken.

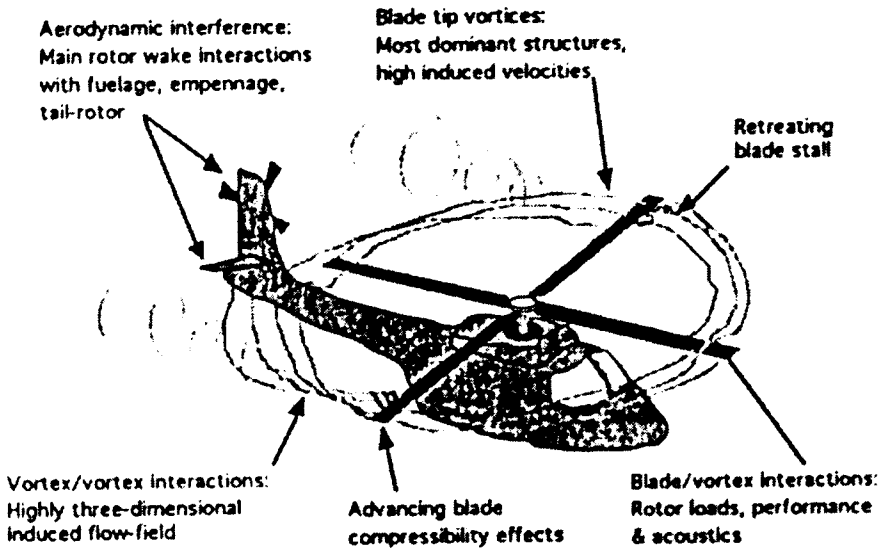


Figure 2-4. Typical Flow Phenomenon Found on a Helicopter in Forward Flight[5]

In attempting to decrease the vortex strength or to change its stability, the most obvious place to start is with the mechanisms of vortex decay that occur naturally. There are three known categories of "natural" vortex decay. The first is viscous diffusion and involves a weak means of natural vortex decay which relies upon the shear between fluid particles to slow the rotational velocities of the vortex to the point where they are no longer strong enough to overcome ambient disturbances. Viscous diffusion generally occurs very slowly, due to the small viscosity of air. It can take miles to dissipate tip vortices produced by large passenger aircraft, assuming other flow instabilities do not accelerate the decay process. The strength and persistence of tip vortices means that this

natural mechanism is generally far too slow to be useful from an engineering standpoint. However, if diffusion can be accelerated, it obviously would be of value in an effort to decrease vortex strength and stability.

The second natural decay process is referred to as vortex bursting. Vortex bursting is characterized by a sudden and violent change in the vortex core flow structure involving tremendous deceleration of fluid particles. This often results in an almost instantaneous dispersion of the vortex flow. This phenomenon occurs only under certain specific conditions – the various combinations of which are not entirely understood. A number of factors are known to influence the likelihood of vortex bursting. These include axial pressure gradient, Reynolds Number, circulation number, geometry of the body, turbulence in the flow and the specific velocity field in question[7]. This method of vortex decay is unlikely to be used for control of tip vortex flow alleviation due to the absence of the required conditions in the subject flow field and because of the difficulties associated with producing the requisite conditions artificially.

The third means of vortex decay is through exploitation of existing flow instabilities, such as the Crow Instability. The Crow Instability is a long wave process characterized by a sinusoidal instability of typically two line vortices that eventually merge, forming a set of vortex rings[8,9,10]. This particular process (active excitation of Crow Instabilities) is also rather slow and requires certain natural conditions for initiation. However, other natural instabilities do exist in vortical flows and have the theoretical potential of being utilized to accelerate vortex decay.

Previous Tip Vortex Control Efforts

It is clear that there are great benefits that can be realized if practical techniques can be found to weaken or to redistribute the vorticity in a body's wake, or equivalently to accelerate the decay of the tip vortices. Efforts to modify the tip vortices shed from wings started almost 75 years ago when end plates were used in an attempt to prevent the

formation of tip vortices[11]. Endplates continued to receive a lot of attention into the early 1950s and met with some success. However, the benefits realized from endplates were tempered by the drag penalty they imposed.

Another moderately successful concept that developed from endplate research was the winglet. Winglets are small lifting surfaces which, when properly designed and positioned on the wingtip, produce a side force which not only serves to inhibit tip vortex formation, but also provides a force component opposing drag. However, winglets can be designed for only one flight condition – typically cruise. Many other non-planar tip geometries have also been evaluated for use on both fixed wing and helicopter blades, generally meeting with only limited sucess[12,13].

Wingtip mass injection is another area that has received recent attention. Lee et. al.[14,15,16] have used a wingtip modified with a long single slot to produce a span-wise jet sheet. The effect of this sheet appeared to have been a modification of the lift distribution similar to that produced by an increase in aspect ratio. Unfortunately, the fundamental nature of the tip vortex for the "modified" wing did not appear to be appreciably altered.

Another technique that has been examined is active excitation of Crow instabilities through external forcing. One such study[8] used oscillating flight surfaces at specific frequencies to excite long wave instabilities. Surprisingly, vortex breakdown occurred before the breakdown mode associated with the Crow instability was observed. Although promising, these methods suffered from having to involve oscillating surfaces typically integral to the operation of the aircraft. This could adversely affect the structure of the airframe and the handling qualities of the aircraft. A more recent computational investigation was conducted by Rennich and Lele[17], which identified another application of the Crow-type perturbation in accelerating the destruction of wingtip vortices. In this particular investigation two smaller vortices were positioned inboard of the main tip vortices in such a fashion that the high strain-rate environment caused perturbations to

grow rapidly. These highly perturbed inboard vortices then imparted large amplitude Crow-type perturbations on the larger wingtip vortices. Both of these "proof-of-concept" investigations highlight the potential of using forced excitation of flow instabilities to accelerate decay. Other means of introducing small perturbations to the flow to affect the vortex stability may be possible.

Basis for Current Research

The foundation for the current study lies in the work performed by Wu and Vakili[8,18,19,20,21], which examined the use of spatially discrete wingtip jets for fixed wing wake vortex dispersion applications. Wu and Vakili have shown that the concept of discrete jets has the potential to effectively disperse the vorticity present in the coherent wingtip vortices. Initial work[8] concentrated on water tunnel tests for flow visualization to qualitatively optimize the effects of the jets. The visual results were dramatic. Blowing with discrete jets clearly dispersed the tip vortex. Figures 2-5 and 2-6 are typical of the results and show the effect of discrete blowing during a water tunnel test of a wing model using dye injection for flow visualization. The mechanism for the change appeared to be the formation of multiple auxiliary vortices that decreased the tip vortex strength and introduced increased instability into the flow field. Further studies were conducted in the UTSI low speed wind tunnel[20]. These tests confirmed the initial results and revealed that the entire flow over the wing was affected. Discrete jets altered the three-dimensional flow field and the lift distribution across the wing. Further, both the water tunnel and wind tunnel studies revealed that the amount of blowing could be optimized for different flow conditions in order to generate maximum effect.

Based upon this work, Matthewson initiated a "proof-of-concept" investigation into the applicability of discrete jets in controlling helicopter blade tip votices[23]. In his studies, he both assembled a rotor test stand (the same test stand used during the current investigation) and conducted initial single component hot-wire anemometry velocity measurements. In particular, Matthewson's results revealed that discrete jet blowing was

very effective in reducing effective velocities in the tip vortices. Figures 2-7 and 2-8, plots of measured effective velocities as a function of time, were typical of the results. In Figure 2-7, the baseline case with no blowing, the standard steep velocity gradients associated with a vortex are visible and are consistent with previous studies[22]. However, in Figure 2-8, where one of the blades was modified for discrete jet blowing, a marked reduction in effective tip velocity was apparent. (The blade phase signal displayed in Figures 2-7 and 2-8 denotes the vortex shed from the modified blade.) In general, the discrete jets provided a comparative 50% reduction in maximum effective velocities. This result alone identified the potential of discrete jets in controlling wingtip vortices.

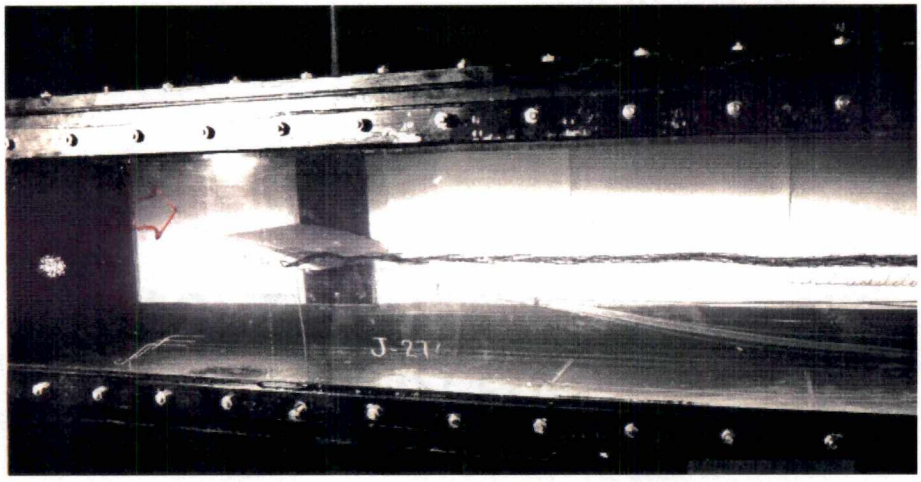


Figure 2-5. Persistent Wingtip Vortex Due to a Lifting Surface – Water Tunnel Dye Injection Flow Visualization[19]

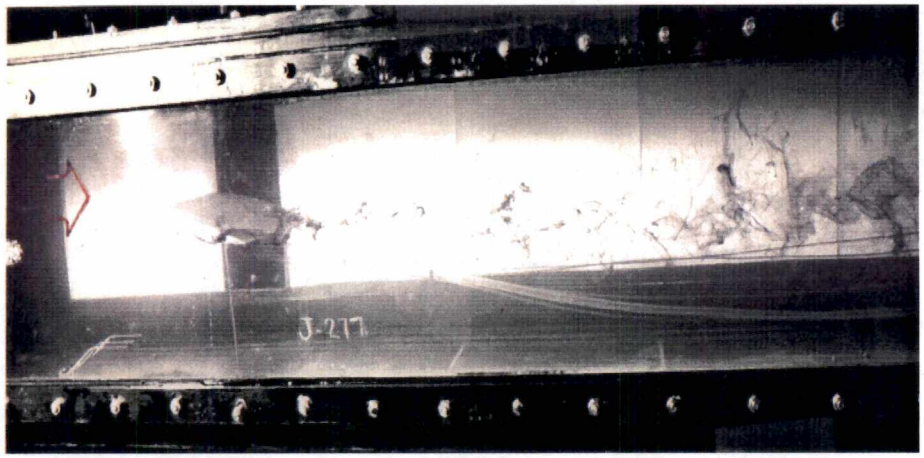


Figure 2-6. Wingtip Vortex Dispersed by Wingtip Flow Control - Water Tunnel Dye Injection Flow Visualization[19]

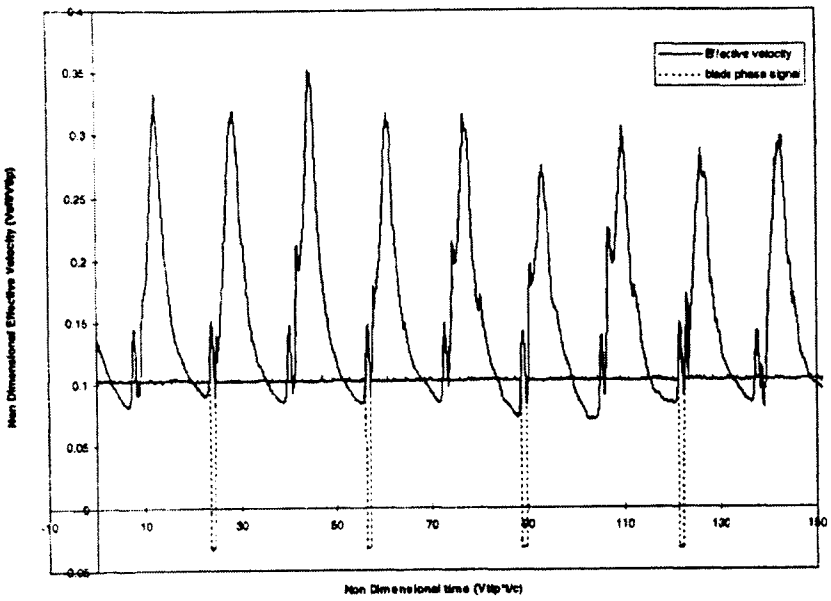


Figure 2-7. Vortex Effective Velocity Ratio vs. Time – Baseline[23]
(No Blowing, peak velocities associated with passage of vortex flow near hot-wire probe)
(RPM = 285, Probe 3" inboard of rotor tip, 1.5" aft of trailing edge plane)

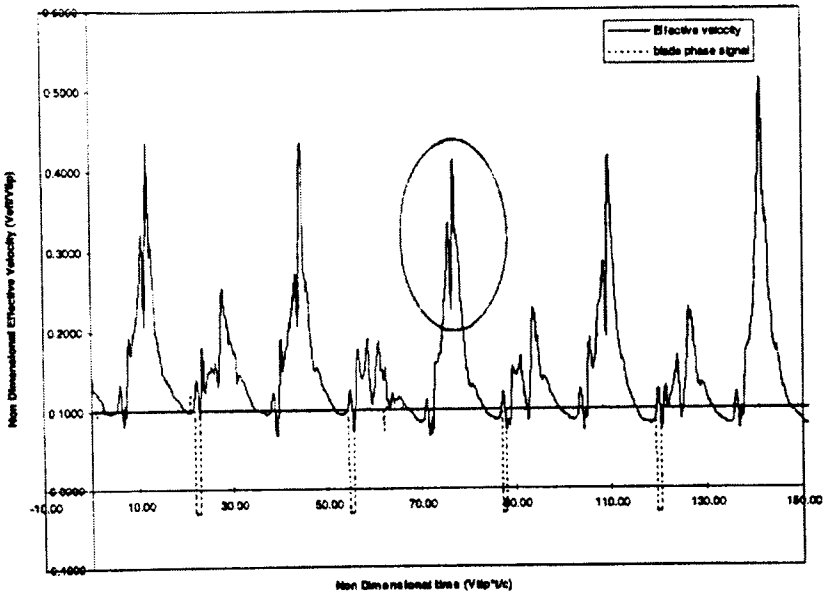


Figure 2-8. Vortex Effective Velocity Ratio vs. Time – 1 Blade Blowing[23]
(Blowing from 1 blade, Cμ=0.0033, RPM = 285, probe positioned as above)
(The encircled area highlights the passage of the vortex core over the probe tip, suggesting satisfactory probe placement in the flow field. The blade phase signal corresponds to the blowing blade, indicating the passage of the 'modified' vortex over the probe.)

It is from this point which the current investigation was initiated. Initially, the work was directed at clarifying the results obtained by Matthewson by conducting near-field flow visualization. Then, additional quantitative measurements were made using Particle Imaging Velocimetry in both the near field and far field for the baseline (no blowing), one blade blowing and two blade blowing configurations.

Dimensional Analysis

The flow field around a helicopter rotor (with and without discrete wingtip jets) is governed by unsteady non-linear equations of motion. In order to gain some insight into the flow dynamics a scaled rotor model was used to represent the full-scale flow. Of course, for the data gathered to be applicable to other investigations the model must be geometrically similar to the prototype and the model flow must be dynamically similar to full-scale flow. To effectively manage all the variables involved in prototype-model comparisons, it is necessary to apply the concepts of dimensional analysis and similitude. It should be noted that since this course of study presented here was research oriented there was no intent for the geometrically scaled model to correspond to a specific helicopter. Nonetheless, by applying a non-dimensional approach to the experiments conducted, a fundamental understanding of the physics of the flow was achieved.

For the case of discrete rotor blade tip jets, the relevant variables were:

Blade Geometry Variables:

- b wing (blade) span
- c wing (blade) chord

Jet Slot Geometry Variables (Figures 3-3 and 3-4 provide a picture and schematic of the jet slots):

- d_s slot width
- L_s slot length

δ_v vertical distance of jet slot centre line above/below the chord line

δ_c distance between jet ports along the chord line

θ_{sweep} sweep angle of injected jet

θ_{di} dihedral angle of injected jet

Jet Fluid/Ambient Fluid Variables:

P_j jet pressure

ρ_a density of ambient air

ρ_j density of jet

μ ambient and jet fluid viscosity

Flow Kinematic and Dynamic Variables:

N rotor frequency (i.e. revolutions per second)

V_{tip} rotor tip velocity

$\dot{m}_j$ jet mass flow rate

V_j jet velocity

f_j jet frequency (cycles per second)

For this investigation, the temperature and density of the jet and ambient fluid (air) were considered to be the same (i.e. there were no significant temperature effects).

The functional relationship between flow kinematics, dynamics and the independent parameters could be thus described:

$$f_1(b,c,d_s,L_s,\delta_v,\delta_c,\theta_{sweep},\theta_{di},P_j,\rho_a,\rho_j,\mu,N,V_{tip},\dot{m}_j,V_j,f_j)=0$$

There were 15 variables in three primary dimensions [M, L, and t]. The Buckingham Pi theorem suggested that a maximum of 12 dimensionless groupings could

be expected to govern this system. By selecting ρ_a, V_{tip} and c as the independent variables representing M, t and L, respectively, the dimensionless groupings could be determined.

As a result, the relationship between flow kinematics, dynamics and the independent parameters could be described in terms of dimensionless parameters as:

$$f_2\left(\frac{\rho V_{tip} c}{\mu}, \frac{b}{c}, \frac{d_s}{c}, \frac{L_s}{c}, \frac{\delta_v}{c}, \frac{\delta_c}{c}, \Theta_{sweep}, \Theta_{di}, \frac{P_j}{\rho V_{tip}^2}, \frac{Nc}{V_{tip}}, \frac{2\dot{m}_j V_j}{\rho V_{tip}^2 S}, \frac{V_j}{V_{tip}}, \frac{f_j c}{V_{tip}}\right)=0$$

In this investigation, the blade and jet slot geometry was fixed by the test stand in use. Also, only steady jets were employed. The pertinent parameters were therefore:

$$f_3\left(\frac{\rho V_{tip} c}{\mu}, \frac{P_j}{\rho V_{tip}^2}, \frac{Nc}{V_{tip}}, \frac{2\dot{m}_j V_j}{\rho V_{tip}^2 S}, \frac{V_j}{V_{tip}}\right)=0$$

By convention, the blowing momentum coefficient was adopted as $C_\mu = 2\dot{m}_j \cdot V_j/(\rho \cdot V_{tip}^2 \cdot S)$, where $S=b \cdot c$. For this investigation the rotor's flow field was a function of Reynolds Number, Jet Pressure Coefficient, Rotor Speed Parameter, Momentum Coefficient and Velocity Ratio. In particular, the Blowing or Momentum Coefficient (C_μ) was used as a key reference parameter between discrete jet investigations.

Chapter III

FLOW VISUALIZATION AND PIV TESTS

Experimental Objectives

The primary objective of this research was to qualitatively and quantitatively assess the potential of discrete jets to control rotor tip vortices. In particular this investigation was conducted to provide greater understanding of the effects of discrete jets on the vortices shed from a model helicopter rotor in terms of velocity and vorticity distribution and general tip vortex trajectory. To achieve this objective, testing was conducted in two phases. First, qualitative data was collected using "smoke" flow visualization. The second phase of testing gathered quantitative data used a new Particle Image Velocimetry system.

General Experimental Set-Up

Test Facility

All tests were conducted at the University of Tennessee Space Institute (UTSI) at the Applied Fluid Dynamics Research Group main propulsion lab.

Rotor Test Stand Equipment

A schematic of the rotor test stand used during all testing is provided in Figure 3-1. The support structure was constructed from steel angle iron and was designed to allow the shaft of the rotor to be 72 inches off the floor (with the rotor disc oriented vertically).

The support structure housed the rotor shaft, variable speed drive motor (1HP capable of 0 to 1700 rpm), jet air supply control equipment, and photo interrupter module.

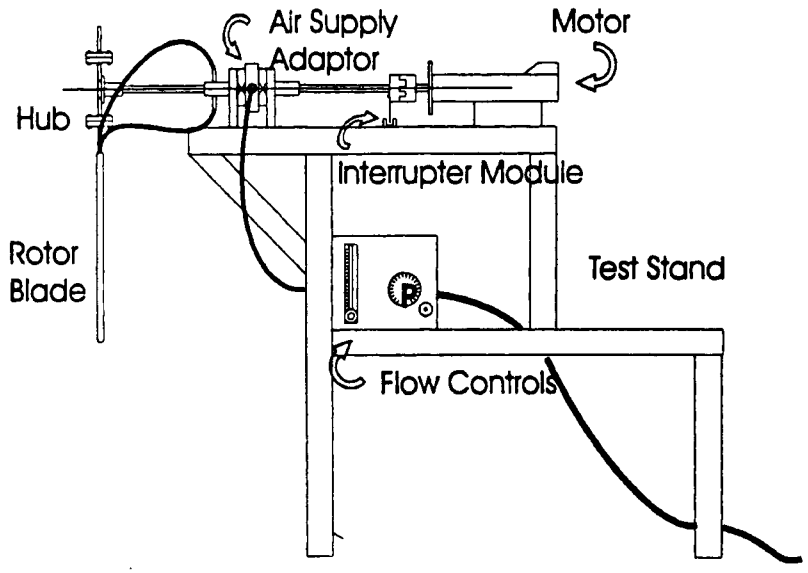


Figure 3-1. Rotor Test Stand Schematic

The two rotor blades were fabricated with fiberglass hand laid-up over a Styrofoam and aluminum skeletal form. A NACA 0012-64 airfoil section was used for each blade. The surfaces were accurate to ± 0.0625". The blades measured 25.25" (semi-span) by 7" (chord). The angle of attack of the blades was manually adjustable via the blade flanges that attached the blades to the rotor hub. Figure 3-2 provides a picture of the rotor hub assembly and rotor shaft bearding/adapter assembly.

Both of the rotor blades were designed with three separate slots at the blade tip to accommodate the discrete jets. Figures 3-3 and 3-4 provide a picture and schematic drawing of one of the blades modified with the jet slots. Air for the discrete jets was supplied to the blade tip through a special supply adapter located in the rotor hub. A pressure regulator and a volume flow rate meter were used to control the air being supplied to the discrete jets in the blade tips. As indicated in the following sections, the configuration of blowing and non-blowing blades (i.e. no blowing, one blowing or both

blowing) was easily achieved by disconnecting/connecting the appropriate air supply lines and blocking/unblocking the jet holes, as required for the particular test condition. It should be noted that, although the blade tips were equipped for blowing out of any or all of the three slots, Matthewson's research revealed that for this particular configuration of slots and blade geometry, the aft most slot (slot #3) was the most effective in dispersing the vortex energy[23].

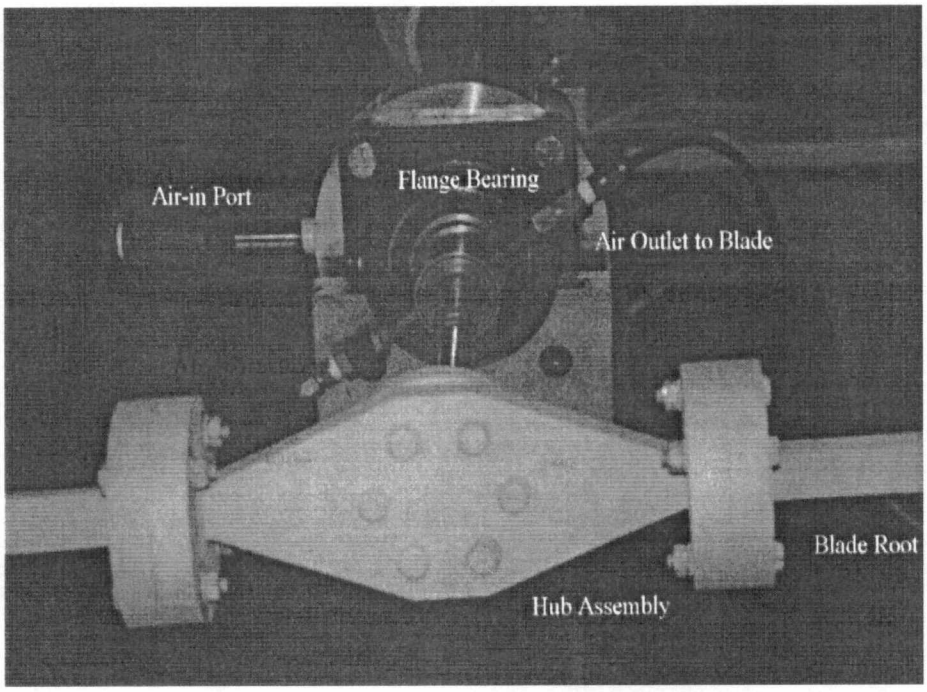


Figure 3-2. Rotor Hub Assembly

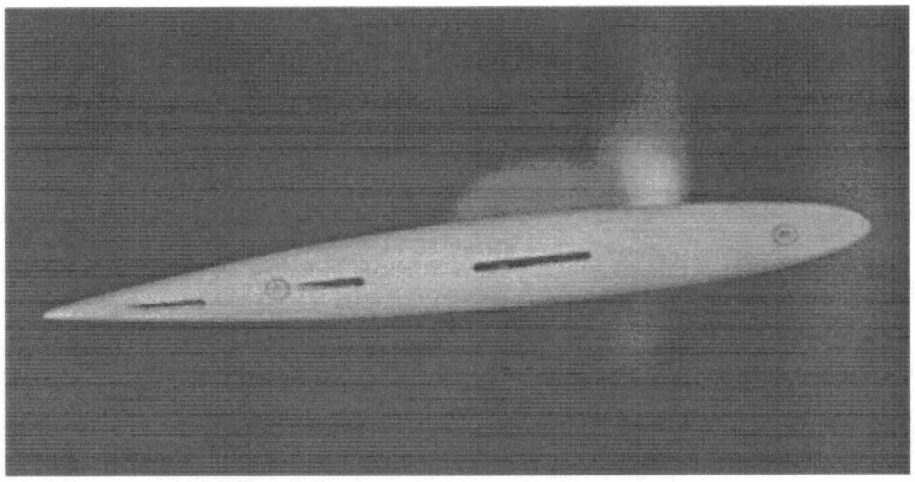
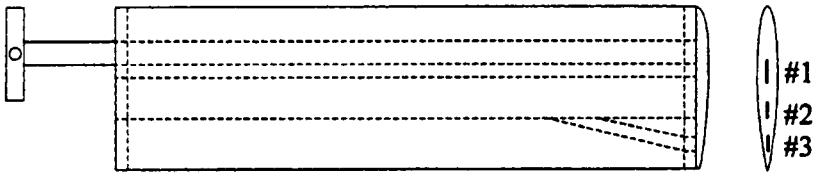


Figure 3-3. Modified Rotor Blade Tip



Blade Data:
Fiberglass skin over foam/aluminum frame with solid aluminum tips
Dimensions: 25 1/4" semi-span, 7" chord
Jet Ports:
#1 : 1" x 5/64" (A_j = .078 sq in), starts 3 11/16" from TE
#2 : 11/16" x 5/64" (A_j = 0.0537 sq in), starts 2 3/16" from TE
#3 : 11/16" x 5/64" (A_j = 0.0537 sq in), starts 3/4" from TE
(#2 directed 30 degree aft (sweep)),
(#3 directed 30 degrees aft (sweep) and 30 degrees down (anhedral))

Figure 3-4. Schematic of NACA 0012-64 Model Rotor Blade

An optical photo interrupter system was used to determine the rotor RPM and to provide blade phase information during flow measurements. A metal tab-plate index was attached to the rotor shaft between the motor and the rotor hub. The tab-plate size and position were set to correspond to leading and trailing edges of one of the blades. The orientation of this tab-plate to a known blade was critical during all tests, but particularly so for the test series with only one blade blowing. The photo-module circuit was triggered by the passage of the tab-plate once per each revolution of the rotor shaft. The RPM measurement was determined by viewing the photo interrupter output signal on an oscilloscope. During PIV testing the blade phase information was also used to trigger laser pulse firings in phase with the rotor, when the rotor blades were oriented vertically.

Flow Visualization Test Set-Up

During the first phase of testing, flow visualization was employed to improve the general understanding of the physics of the flow field as well as to help prepare for future down-stream velocity measurements. The visualization itself was achieved using the

smoke particle injection method. A commercial grade smoke generator supplied atomized oil through a two-inch diameter stainless steel flexible pipe. This output pipe was stepped down to a ½" PVC pipe for localized "point" smoke insertion into the blade-tip flow field. An aluminum box 5" X 5" X 18" 'settling' chamber with an integrated fan assembly was fabricated and placed between the exit of the smoke generator and the ½" output PVC pipe to allow satisfactory and uniform smoke supply. A picture of the smoke flow visualization set up is provided in Figure 3-5.

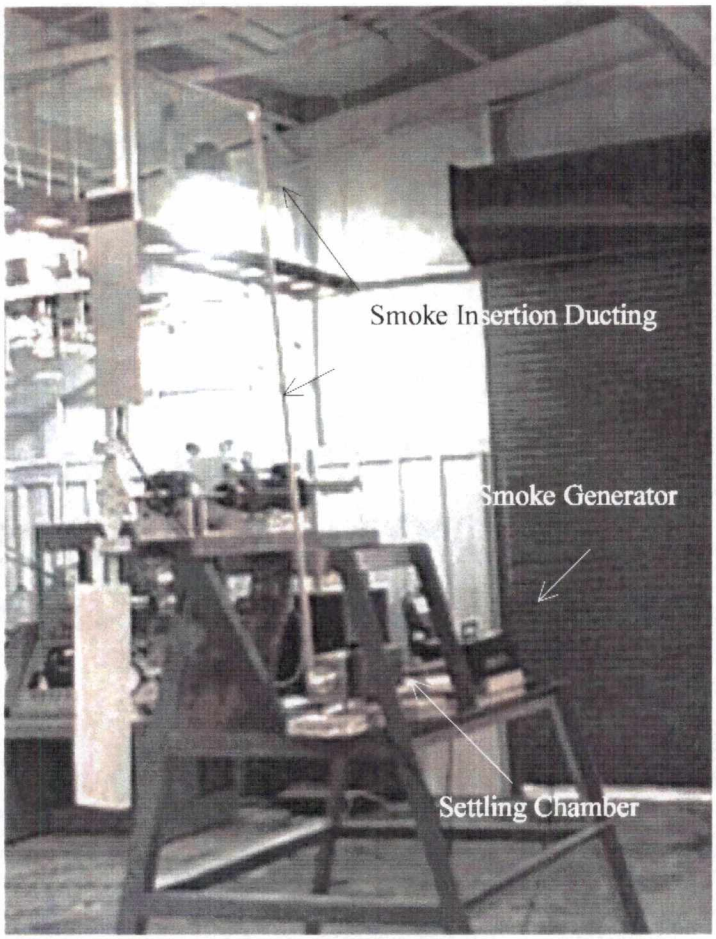


Figure 3-5. Flow Visualization Set-Up

To minimize the influence of the stand structure on the flow, the flow was seeded and captured on video at the top of the rotor disk (i.e. the 12 o'clock position). A high power halogen light source was used to illuminate the smoke particles against a marked black background. The visualized blade tip wake flow, including the blade tip vortices,

were recorded using a VHS video camera for post-test review and analysis. Selected images have been digitally recorded and are used in the later parts of this paper. The physical orientation of the camera, test stand and light source remained constant during all flow visualization tests.

Flow Visualization Test Conditions

All flow viz. tests were conducted at a rotor angular velocity of 200 rpm (providing a tips speed of approximately 7 feet per second) as determined from the photo-interrupted module information displayed on an oscilloscope. Although the angle of attack was initially planned to be a constant 5° (with the relative flow into the test support stand) initial efforts revealed that an angle of attack of -5° (flow away from the test stand) would be more convenient for visualization of results. For the visualization tests involving tip blowing, a jet momentum coefficient of $C_\mu = 0.0774$ was used. Only jet slot #3 (nearest the trailing edge) was used during this portion of testing. The jet air pressure was maintained at 15 psig to prevent air supply adapter and bearing leakage problems. The Reynolds Number (based on tip speed and chord length) for all the flow visualization tests was approximately 0.3×10^6. Flow visualization data was collected for two blowing configurations: the baseline case with no blowing and the "modified" case with one blade blowing. The flow visualization image field of view was oriented such that the three vortices nearest the rotor disk (the vortices from the previous 1 ½ revolutions) could be viewed.

PIV Test Set-Up

In order to broaden the understanding of the effects of discrete blowing on the rotor tip flow field, Particle Image Velocimetry (PIV) was used during the second phase of testing. Due to PIV's relative complexity, prior to discussing the actual system set-up

during this test, a brief overview of PIV will be provided. Following the review, the components of the PIV system will be described.

PIV makes it possible to observe velocity fields typically of two-dimensions on a planar domain at one instant in time. In essence PIV processing is basically determining the distance that seeded particles in the flow field have moved in the time between two laser pulses that serve to illuminate the particles in the flow field for an image capturing device. In this investigation's particular application, 2-Frame Cross Correlation was the method used to determine the velocity vectors from the images taken. 2-Frame Cross Correlation uses two image frames and two laser pulses with one pulse of light (and therefore one image of the flow field) in each frame. In the case of this investigation, a constant pulse separation of 150 μs was used during all tests. This pulse separation allowed for adequate differences in the images to allow reasonably good correlation of particles. The flow field velocity was then determined by measuring the distance the seeded particles have traveled from the first to the second frame[24]. 2-Frame Cross Correlation has several advantages over other methods available (Single Frame Cross Correlation and Auto-correlation) since it allows the velocity to be measured without any directional ambiguity, thus negating the requirement for image shifting and thereby allowing more direct measurement. Further, 2-frame cross correlation data has the best signal-to-noise ratio of all the techniques, since particles are not repeated upon the same image.

Twin Continuum Surelite I-10 Nd:Yag Lasers with a rated output of 205mJ and 205 watts at 532nm generated the laser pulses used during this test. Both cylindrical and spherical lens optics were required to generate and properly orient a laser light sheet from these lasers (as detailed in the following paragraph). The images of the seed particles illuminated by the Nd:Yag lasers were captured by a TSI PIVCAM 10-30 CCD camera with a 60mm FL F/2.8 Micro Nikkor Lens for wide field of views and a Nikon Series E 70~120mm Zoom Lens for close up images. The lasers and CDD camera were controlled through a TSI Model 610032 LaserPulse Synchronizer. The synchronizer was

linked to a Pentium II 233 MHz personal computer equipped with Windows NT 4.0 and TSI Model 600031 Insight NT Software. The TSI Insight software presented a simple graphic user interface which allowed the operator to easily define all laser, camera and data recording options, as required. The Insight software also allowed for image spatial domain calibration so that the calculated velocity vectors could be expressed in useful engineering units (m/s). The TSI LaserPulse synchronizer was also connected to the optical photo interrupter, thereby allowing the laser pulses to be indexed to a particular blade angle. A photo of the PIV set up is provided as Figure 3-6. A complete technical description of and operating instructions for the TSI LaserPulse Synchronizer and PIVCAM 10-30 is provided in the TSI Model 610032 LaserPulse Synchronizer Instruction Manual[25].

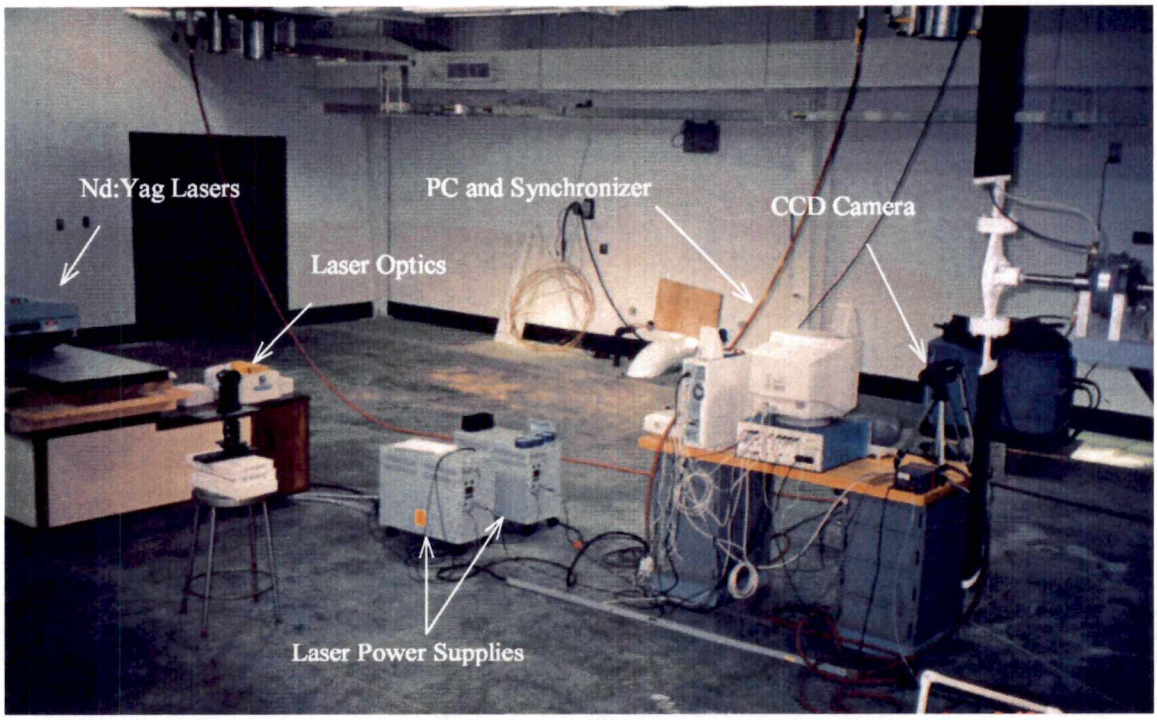


Figure 3-6. Lab Set-Up for PIV Tests

In order to generate a light sheet from the laser pulses produced from the Nd:Yag lasers, two separate optic elements were required. First, a 50mm Half-Round lens was used to project a vertically oriented light sheet from an incident coherent laser beam. Then a 2000mm focal length spherical lens was used to ensure proper laser sheet

convergence at the point where the CCD camera was focused. The half-round and spherical lenses were collocated in one optic mount, which was positioned 2 m from the area of interest.

Flow Seeding

In any PIV measurement, the type of seeds particles used and the means by which they are inserted into the flow field are critical to the success of that measurement. For this investigation, two different seed particles (atomized oil and atomized water) were evaluated for suitability in the rotor tip vortex application. Further a variety of seeding locations, including point insertion methods and sheet insertion methods were examined. Both the documentation shipped with the TSI PIV system[24] and work developed by Melling and Whitelaw[26] identified some of the background concerns involving the seeding of gas flows. Some general strategies for imaging flow fields with PIV systems were also provided by Adrian[27]. These works should be consulted for further detail, as required.

The first method of particle seeding investigated utilized atomized oil generated from the same commercial smoke generator as used during flow visualization tests. However, it was found that the small aluminum-settling chamber used during flow visualization tests was inadequate for producing the uniform concentration of particles required for PIV. A larger settling chamber was thus constructed from a 30-gallon cylindrical plastic tank. The smoke was feed into the chamber through a valve assembly at one end. The smoke supply valve assembly was then closed and the smoke was ejected through the ½" PVC output pipe with pressurized shop air. Figure 3-7 presents a photograph of the smoke generator and 30-gallon settling chamber. From the ½" PVC output pipe, various insertion methods were attempted. Initial tests used a "point" insertion method with the smoke entering the flow field directly from the end of the ½" PVC pipe at a distance of approximately 6" behind the rotor disk at the 6 o'clock position. A second and more effective method of insertion utilized a manifold (depicted

in Figure 3-7) which allowed the smoke to be issued in a "sheet". It was found that the best PIV results were obtained with the smoke "sheet" being issued 8 inches below the rotor disk at the 6 o'clock position. This latter configuration using atomized oil was eventually adopted for all PIV tests.

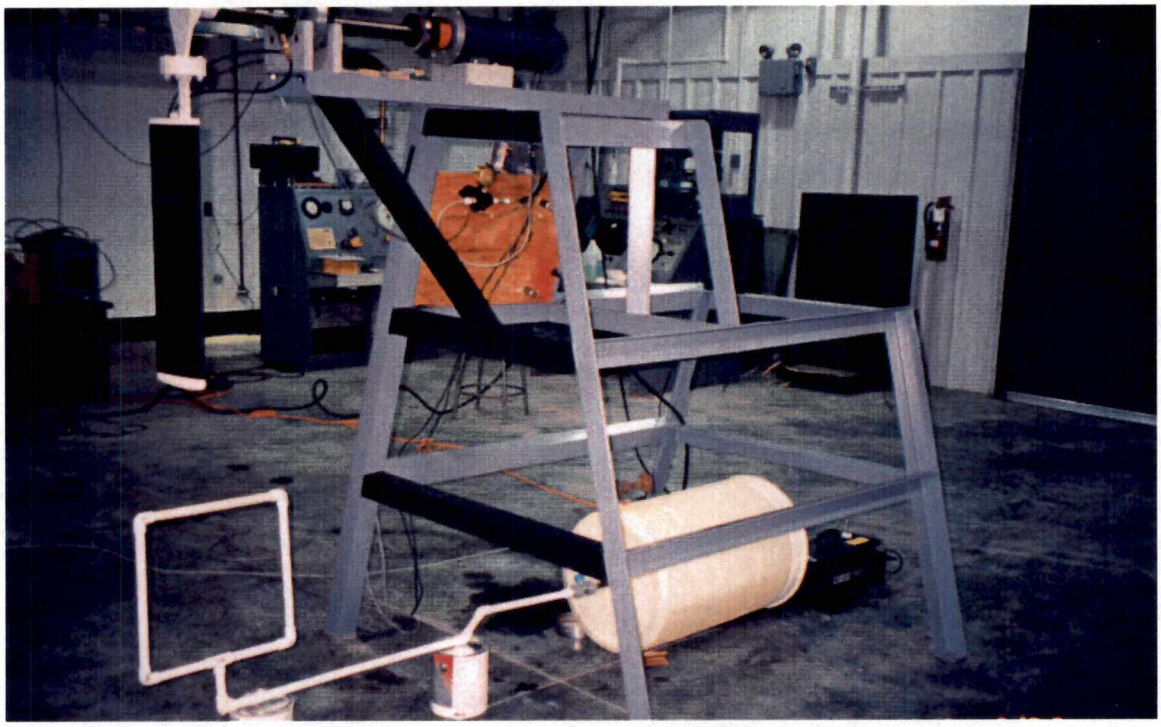


Figure 3-7. Smoke Particle Generation and Insertion Apparatus

The second type of seed particle investigated for use with the PIV system was atomized water. A six-jet atomizer, modified to issue air/water out of only two holes was used to inject the atomized water particles. High-pressure air (approximately 100 psi) was mixed with a low flow rate of water (approximately 0.5 gph) to produce a fog. Unfortunately it was found that there was insufficient air pressure to produce the appropriately sized particles necessary for good PIV data collection in this application.

PIV Test Conditions

As was the case with the flow visualization tests, the PIV tests were conducted so that direct comparisons could be made between test points to identify the effects of blowing from one blade and both blades in both the near field and the far field. Table 3-1 presents a summary of the test points evaluated during the PIV testing. It should be noted that since the laser was synchronized to the blades being located in a vertical position, the images of the tip vortices at the 6 o'clock position were identified by "the number of revolutions" downstream of the rotor disk. For example, the tip vortex being shed at the instant the image is captured would be visualized at the blade tip, whereas the vortex shed half a revolution earlier would be visualized directly next to that "current" vortex, and so on. This method of identifying vortex position is used throughout this document.

Table 3-1. PIV Test Matrix

PIV CCD Camera Area of Interest	**No Blowing**	**1 Blade Blowing**	**2 Blades Blowing**
Near Field (Vortex ½ Rev. from Rotor Plane)	**X**	**X**	
Near Field – Wide View (Both the vortex currently being shed and the vortex shed ½ rev. earlier)	**X**		**X**
Far Field (Vortex shed 2 ½ revolutions ago)	**X**		**X**

During PIV testing, the rotor was operated at an angular velocity of 240 RPM (providing a blade tip speed of approximately 8.4 feet per second). For all PIV tests, the rotor blade angle of attack was -5° with the flow moving away from the rotor stand. For those series of tests that involved blowing from one blade, the jet air supply tubes were directed to port #3 of the blowing blade. This resulted in a net blowing coefficient ($C\mu$) of 0.0255. For those series of tests that involved blowing from both blades, jet slot #3 was used on each blade. For these tests the jet air pressure and volume flow rate was increased slightly to make up for the relative increase in jet slot area (for two blades),

resulting in a blowing coefficient ($C\mu$) of 0.020 for each blade. The overall Reynolds Number (based on rotor tip speed and blade chord length) for all tests was 0.6×10^6.

It should be noted that prior to all tests the CCD camera was spatially calibrated using the TSI Insight software. This calibration was conducted to allow the PIV data to be easily expressed in standard engineering units of m/s. This calibration also allowed direct relative comparative measurements of vortex core displacement or movement when blowing was applied from one or more blades between all PIV results.

Chapter IV

RESULTS AND DISCUSSION

Flow Visualization Results and Discussion

Two main test configurations were examined during flow visualization testing. First, baseline flow visualization was carried out without any discrete jet injection (no blowing). Figure 4-1 documents the structure of a typical tip vortex for this case. As expected, the vortices generated moved radially inward from the blade tip (i.e. towards the rotor centerline). When flow visualization was conducted with discrete injection from one blade tip a slightly modified flow pattern was revealed (Figure 4-2). It should be noted that for the vortices pictured in Figure 4-2, only every second vortex corresponds to the blowing blade, as denoted in the image. By comparing a series of flow visualization images, the trajectory and the apparent structure of the tip vortices could be determined for the blowing and non-blowing cases.

The most obvious trend difference witnessed was the change in the path of the vortex shed from the modified blade. Initially, the vortices shed from the modified blade were displaced slightly in the outward radial direction (up in the image) as compared to the baseline case. Then, as the vortex traveled downstream, they moved radially inward of the "baseline vortices". This observation was in agreement with previous water tunnel flow visualization tests conducted by Matthewson[23] for a fixed wing with discrete jets. Matthewson's fixed wing flow visualization revealed that as the vortices shed from the modified blade moved downstream, they also exhibited a tendency to move radially inward. This radial inward motion appeared to be greater for the 1 blade blowing case than for the baseline case.

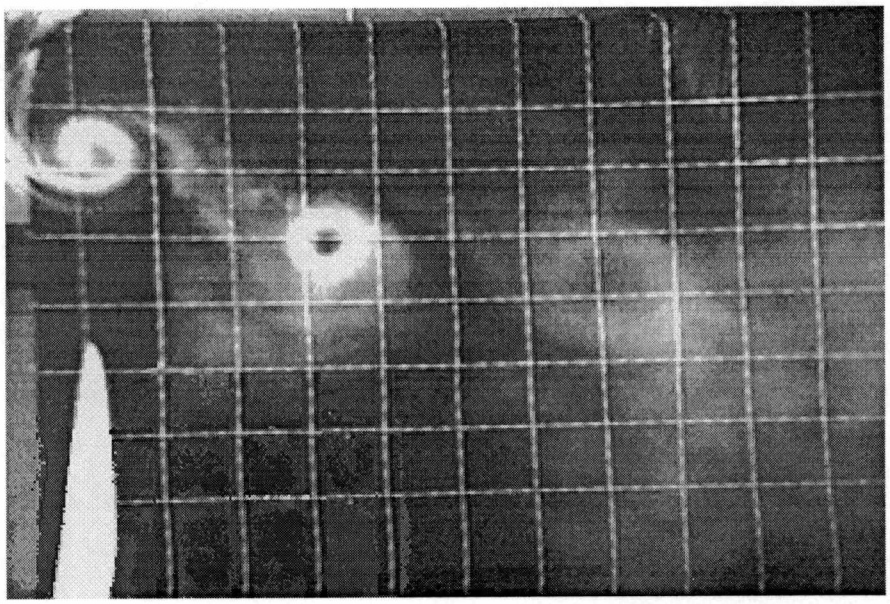


Figure 4-1. Smoke Flow Visualization (No Blowing, RPM = 200)

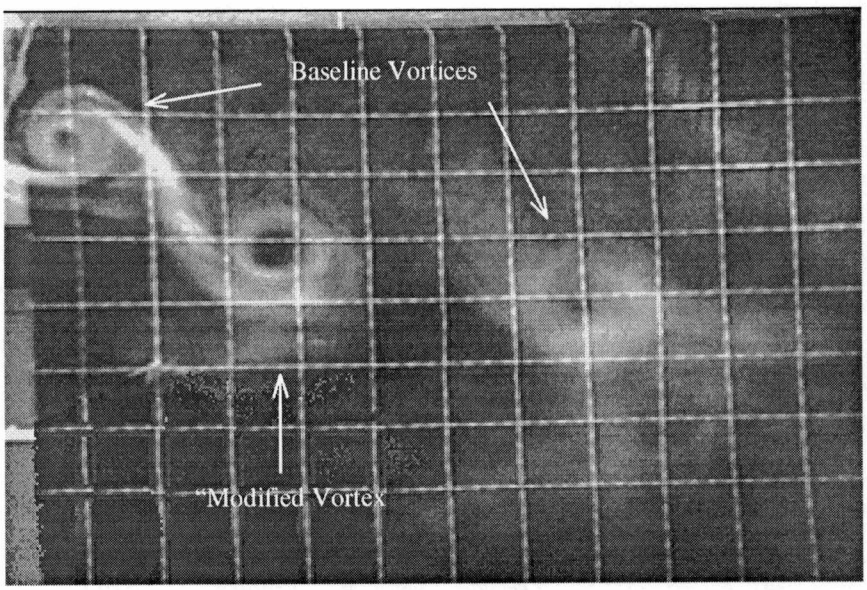


Figure 4-2. Smoke Flow Visualization (1 Blade Blowing)
(Cμ=0.0774, RPM=200, Viewing Angle is same as Figure 4-1)

The vortices shed from the modified blade tip appeared to have some other unique characteristics. The core of the vortex generated by the modified blade appeared to be less concentrated than that shed from the baseline blade tip. This observation was evident when the relative vortex "core" size was compared between the blowing (Figure 4-1) and no-blowing (Figure 4-2) cases for vortices at the same relative spatial location.

Further, the vortices shed from the modified blade appeared to dissipate more quickly than those shed from the baseline blade in the far field (beyond that field of view of the camera used during flow visualization).

During the conduct of flow visualization testing, an interesting collateral observation was made. While first setting up the no blowing test, with the rotor blades inadvertently configured with slightly disparate angles of attack (-5° on one blade and -4° on the other) a form of vortex merging was observed. Figure 4-3 provides an example of such a case. It was observed that as the variation in angles of attack increased the merging tendency of the tip vortices increased (i.e. they rolled up more quickly with larger difference in angle of attack). This observation obviously had some value in the field of vortex merging. For the current investigation however, the objectives were to study the effects of discrete jets on tip vortices for a rotor in hover. Therefore, the merging tendency was minimized to the greatest extent possible.

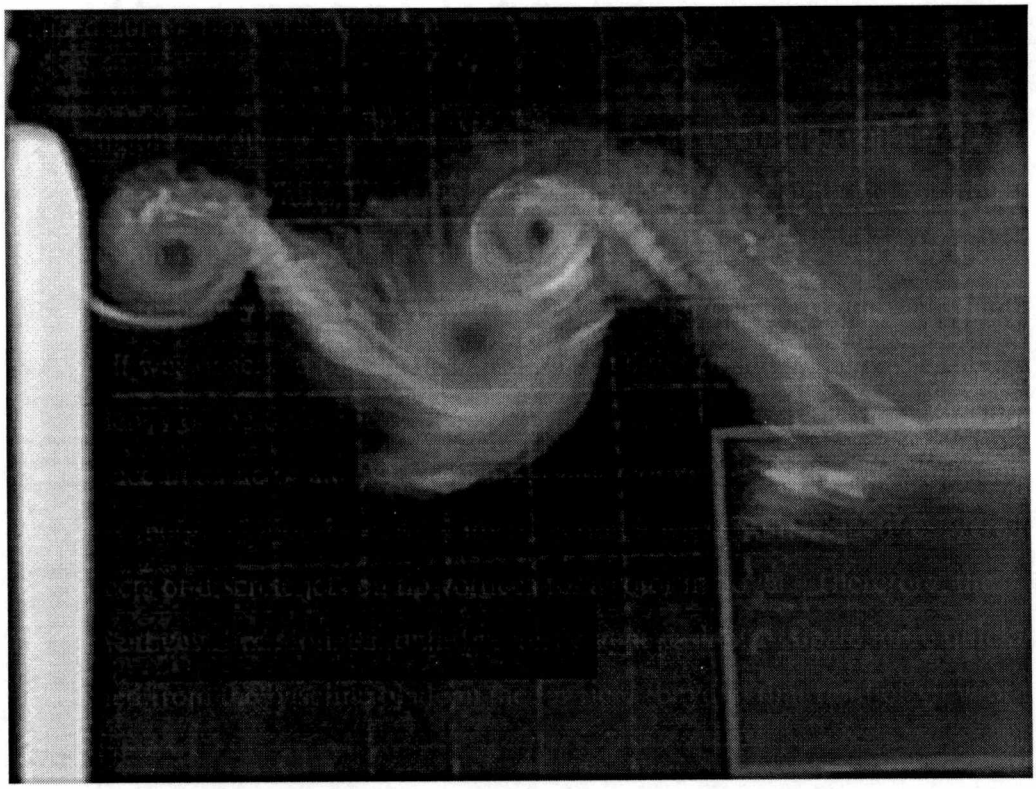


Figure 4-3. Vortex Merging (No Blowing, RPM = 200)

PIV Testing Results – Post Processing

In Chapter III the basic nature of PIV was discussed. In particular the 2-Frame Cross Correlation system employed during this specific PIV test was briefly explained. However, once the images were acquired and the cross correlation was conducted, significant post-processing was still required to develop meaningful results. This post-processing was required for many reasons, not the least of which was related to the difficulty experienced in adequately seeding the flow field. During testing it was realized that full flow field seeding would be nearly impossible for all flow conditions – the result being that there were occasional data point "drop-outs". As a result some post-processing was required to remove/replace the erroneous vectors which these data "drop-outs" created. The following paragraphs briefly summarize the post-processing activities that were used to generate the PIV data presented in this report[28]. The post-processing software used for this purpose was provided by TSI and was a "Beta" or test version of EditVec, a software package being developed specifically for use with their PIV systems.

Figure 4-4 presents a typical raw data set (for a baseline, no blowing, case) generated by the TSI Insight software application after correlating the two images of the flow field. As with all PIV data presented here, the image plane is oriented vertically, perpendicular to the rotor disk and intersects the rotor hub. The y-axis in the PIV images corresponds to the vertical "up" axis of the plane and the x-axis corresponds to the horizontal "downstream" axis. Obviously, there was some data lost due to imperfect flow seeding. The most obvious errors are the erroneous velocity vectors located below the 75mm point on the Y-axis, which corresponds to area outside the cylinder formed by the vortices shed from the rotor. (It should be noted that the axis scales are accurate, however, their absolute distance is meaningless – i.e. the 75mm position is referenced only to the bottom of the CCD camera's field of view.) Also, near the top of the vector plot, there are two more dropped data points, indicated by the white blocks. In order to remove the obviously erroneous data and smooth the occasional dropped data point three post-processing tasks were conducted. First, the data set was passed through a Range

Filter. The purpose of the range filter was to remove the conspicuously erroneous data. The range filter was set to ± 7 m/s – so that any velocity vector in excess of ± 7 m/s would be removed. The range filter was applied specifically to remove those data points outside the main flow field where seeding was generally poor. Figure 4-5 illustrates the results of passing the raw data set through the range filter.

The remaining two post-processing activities were aimed at correcting the occasional dropped data point "inside" the flow field. The second filter used (after the range filter) was a local median filter. The local median filter compared each velocity vector to the median value of the surrounding neighbourhood vectors. The median value was found by sorting the neighbourhood vectors U (i.e. in the x-direction) components in ascending order. The middle value in the sorted velocity component array was the median. The median was then calculated for the V velocity component. The tolerance of the local neighbourhood filter was set to 2m/s. The neighbourhood size was set at 5 X 5 vectors. Figure 4-6 shows the sample data set after being passed through the local median filter.

The final filter, through which the data was passed, was a smoothing filter. The smoothing filter replaced each velocity vector with a weighted average of a velocity vector and its neighbouring vectors. The smoothing filter was designed to filter out high frequency velocity variations caused by the uncertainty in measuring the velocity with a PIV system. A Gaussian weighting array was used to determine the amount of weighting to be applied to each vector in the neighbourhood being examined. The center of the weight array was the vector itself and was given a weighting of 100. A small neighbourhood of 3 X 3 vectors was used to minimize the amount of smoothing provided by this filter. Table 4-1 details the Gaussian weightings provided by the smoothing filter in the 3 X 3 neighbourhood. Figure 4-7 illustrates the effects of the smoothing filter on the sample data set.

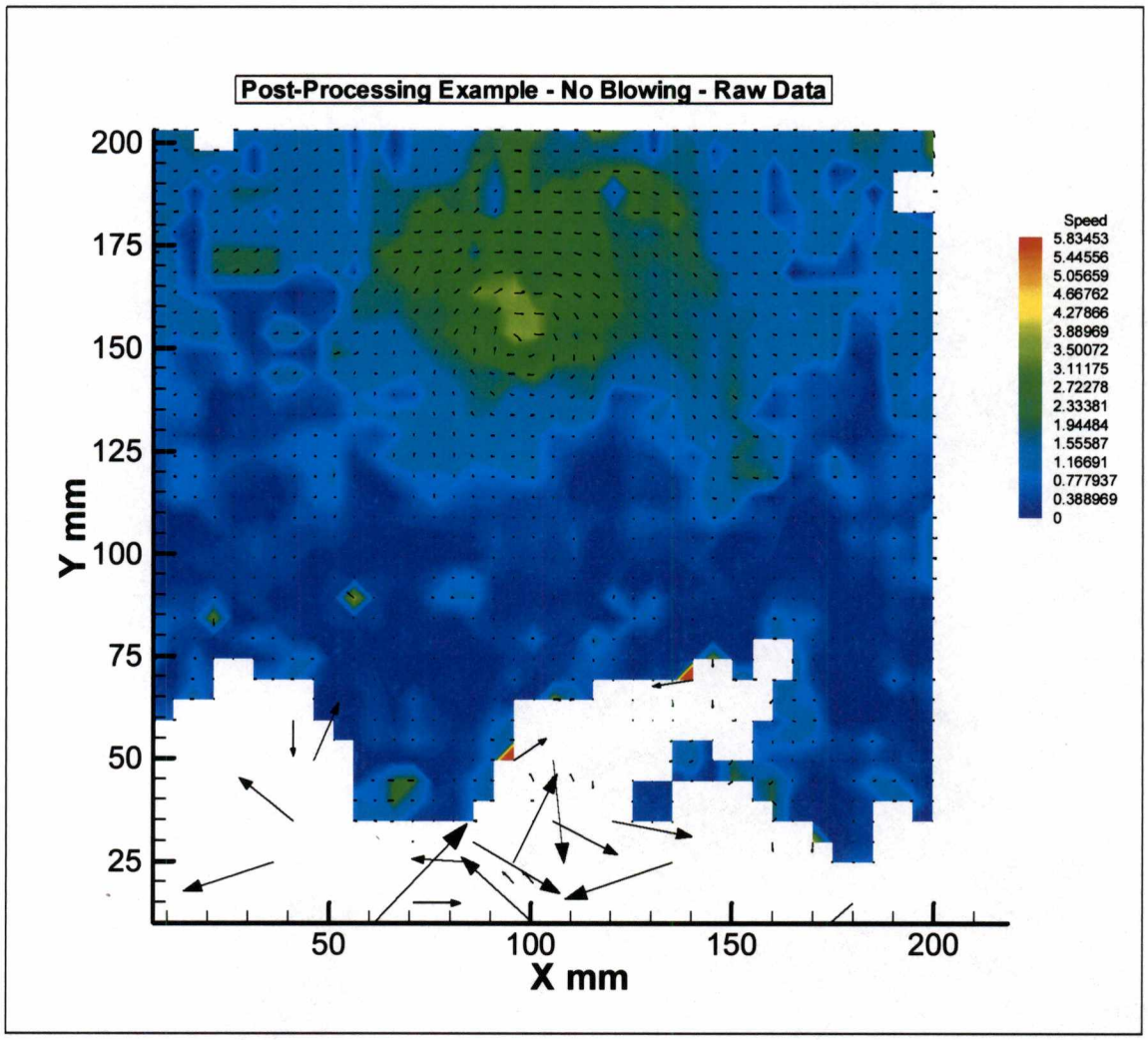


Figure 4-4. PIV Test Data Post-Processing Example of Raw Data

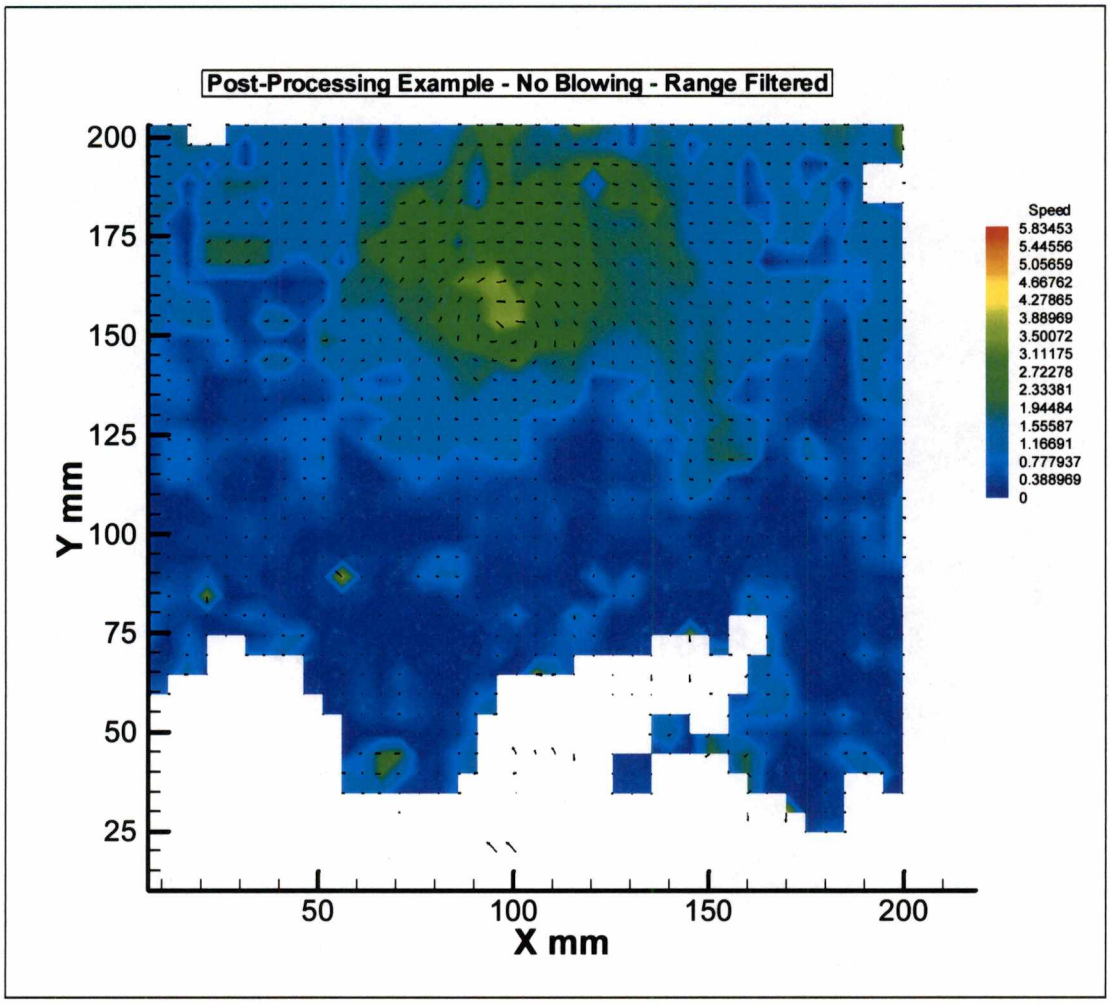


Figure 4-5. PIV Test Data Post-Processing Example of Raw Data with Range Filter Applied

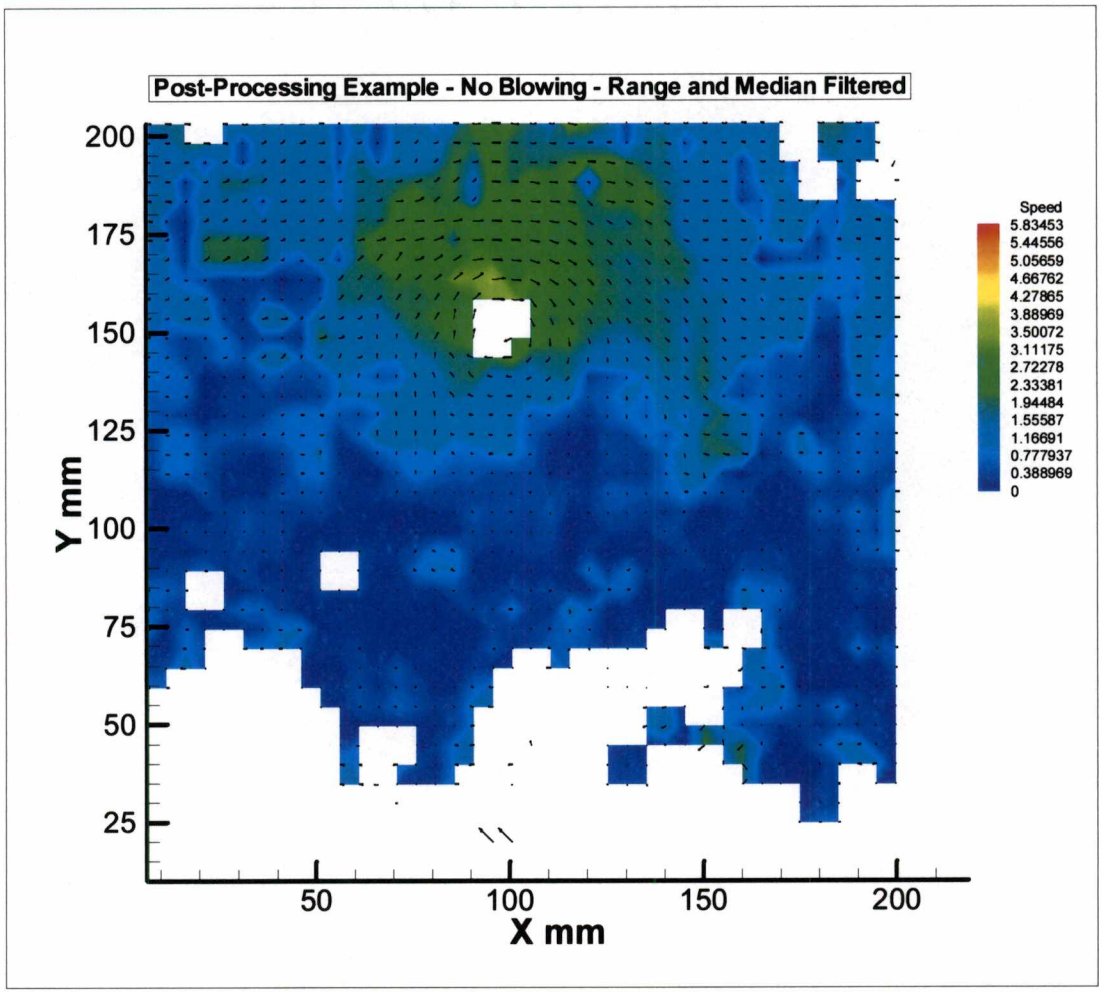


Figure 4-6. PIV Test Data Post-Processing Example of Raw Data with Range Filter and Median Filter Applied

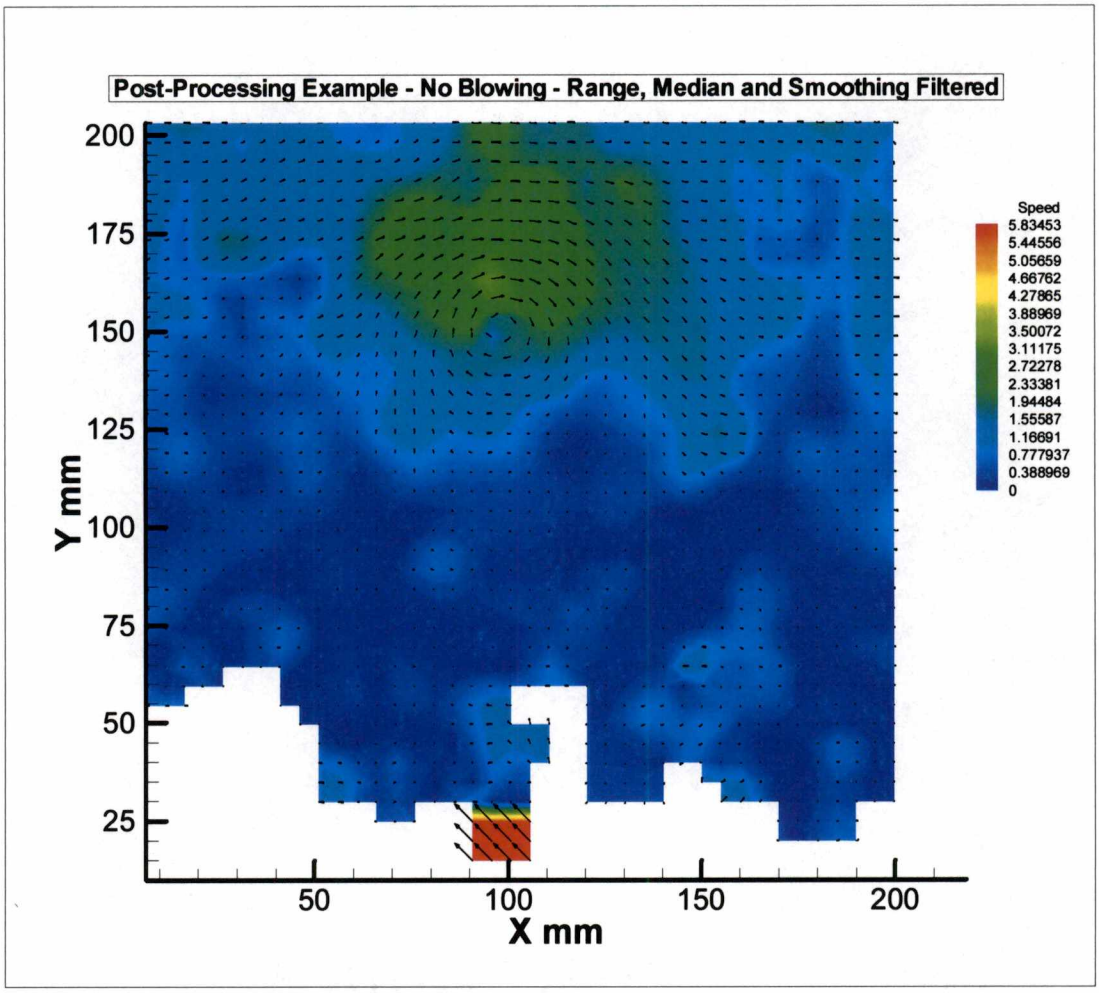


Figure 4-7. PIV Test Data Post-Processing Example of Raw Data with Range Filter, Median Filter and Gaussian Smoothing Applied

The net effect of applying these three filters can be observed by comparing Figures 4-4 and 4-7. In general, the specific area of interest (the vortex and the immediate surrounding flow field) was unchanged, except for minor smoothing of the velocity peaks near the vortex core. At those points where occasional data drop-outs occurred, their values were satisfactorily interpolated. As well, where poor seeding resulted in obviously erroneous values, the filters minimized their impact on the image as a whole.

Table 4-1. 3 X 3 Neighbourhood Gaussian Weightings

27	40	27
40	100	40
27	40	27

The remainder of the results presented within this thesis will be of post-processed data. The specific conditions of the filters are the same as those specified above. Except as noted in particular discussions, all data presented herein were phase-averaged results of several images.

Additional post-processing of the data was conducted to calculate local values of vorticity from the velocity vectors generated by the PIV tests. The vorticity was simply obtained by numerically calculating the local strain rates and then determining the vorticity [½ (dv/dx-du/dy)].

PIV Test Results and Discussion

Six sets of data and over 1500 images were collected during PIV testing. The first test condition evaluated was that of the baseline case in the near field, with the area of interest being the vortex located ½ revolution downstream. Figure 4-8 provides the resulting vector field and velocity contours. As was expected the maximum velocity in the flow field occurred above the vortex core; at this position the vortex rotational

velocity is combined with the vortex translational (downstream) velocity. Figure 4-9 is the same test condition but expresses the results in terms of vorticity.

In comparison, the PIV results for the same spatial location with blowing from one of the blades (corresponding to the vortex in the field of view) revealed some significant differences. Figures 4-10 and 4-11 present typical velocity and vorticity contours, respectively, for the same near field position with one blade blowing. From direct comparison between the vorticity contours, it was obvious that the blowing had displaced the vortex core radially outward in the rotor's frame of reference (or in the frame of reference of the vector plots, downward). Furthermore, based on a comparison of the velocity contours, it was apparent that the velocity in the 1-blade blowing case was not as concentrated at the vortex core as with the baseline case. Higher flow speeds were visible further away from the vortex core in the blowing case. This observation was very significant, since it indicated that the velocity of the vortex was being distributed away from the vortex core. The distributed velocity meant that a lower velocity gradient existed near the vortex and, given the direct relation to sound pressure level to velocity gradient, this "modified" vortex would impart less impulsive noise in the event of a vortex-blade collision. Reviewing the respective vorticity contours (Figures 4-9 and 4-11) further substantiated this observation. In these figures the vorticity gradient near the core appeared to be less for the blowing case as compared to the baseline case indicating a less concentrated vortex. Further, based on the vorticity contours, the vortex core of the 1 blade blowing vortex appeared to be much less symmetric than that for the baseline case. It should be noted that giving consideration to Kelvin and Helmholtz's theorems, the observed data suggested an increased rate of dispersion of the vorticity (instead of destruction of vorticity) was occurring because of the discrete jet blowing. Further, the results obtained by Vakili and Wu[18,19,20,21] indicated that the lift distribution of a fixed wing was positively effected by the use of discrete jets. Therefore it is likely that, in fact, more total vorticity is present in the flow field for the blowing case even though it is less concentrated as compared to the baseline case.

To further emphasize the effect blowing has on the structure of the tip vortex, a second series of PIV tests, consisting of a near field area of interest with a wide view of the flow field were conducted. This wide view allowed simultaneous viewing of the first two vortices shed from the blades. As indicated in Table 3-1, the baseline case and the 2-blades blowing case were evaluated for this area of interest. The overall quality of these images and the resulting data were not quite as good as for the previous series. The decrease in data quality was attributed to the fact that with the larger field of view, larger portions of the flow field and areas outside of the flow field (where seeding was impractical) were evaluated. Notwithstanding this problem, based on a comparison of the velocity profiles for the baseline case and the 2-blades blowing case (Figures 4-12 and 4-13, respectively) similar observations could be made regarding the effectiveness of the tip vortices. For the case with two blades blowing, both tip vortices demonstrated a broadened velocity gradient indicating increased diffusion of energy into the flow field. As before this diffusion of velocity suggested that the "modified" vortex would impart less impulsive noise if it were to collide with a rotor blade or other structure. The comparison of the velocity contours also suggest that the vortex located ½ a revolution downstream for the blowing case did not experience a change in trajectory such as that witnessed for the one blade blowing case previously discussed. It is possible that when only one blade is blowing and the other is not, some form of interaction occurs between the vortices, causing the change in trajectory. (Recalling that small differences in the rotor blade angle of attack caused the tip vortices to merge, it is conceivable that the mixed blowing-non blowing condition could cause a change in vortex trajectory.) During the testing, "real-time" observations of the two-blade blowing configuration revealed that the shed vortices also had a tendency to "wander" slightly. It is possible that this small amount of wandering may have hidden a change in trajectory, if it occurred. Further testing, with improved seeding methods should clarify this dilemma. It should be noted that although the amount of vortex movement was small, all data presented for the 2 blade blowing configuration is for specific (but typical) sets of data collected in lieu of averaged data (such as is presented for the no blowing

configurations). This consideration was made to ensure details of the flow field were not "averaged-out".

In order to determine the far field effects of discrete jets on the vortices shed from a rotor blade, far field PIV measurements were also conducted. Up to this point in testing, the flow seeding method was marginally satisfactory to provide reasonable PIV results. However, in the far field tests, many more data points were required to be collected to ensure accurate observation since the seeding method was critically deficient. Further, the unsatisfactory seeding capabilities required that the far field tests be conducted relatively close to the rotor disk. The far field images presented here were of the vortex corresponding to a position 2 ½ revolutions downstream. Figures 4-14 and 4-15 provide a sample of the far field data observed for the baseline case and the case with 2-blades blowing. The differences between the two were readily apparent. Compared to the baseline configuration a complete vortex structure was not readily visible in the 2-blade blowing case. Further, if a comparison of approximate vortex core size is made between the near field results (Figure 4-8) and the far field results (Figure 4-14) for the baseline configuration alone, it is apparent that the "baseline vortex" has only increased slightly in size. The effectiveness of discrete jets in accelerating vortex decay is obvious. It should be noted that in Figure 4-14, it appears as if a solid wall is located at the 100mm point along the y-axis (parallel to the x-axis). This vector representation is a result of the influence of the poor data (i.e. poor flow seeding) which was collected outside the direct rotor flow field. The post-processing functions amplified some of these errors in the lower portion of this image, causing the effect witnessed. This error was allowed to be included in this report, due to the difficulty in obtaining suitable data at the far field location, as previously mentioned.

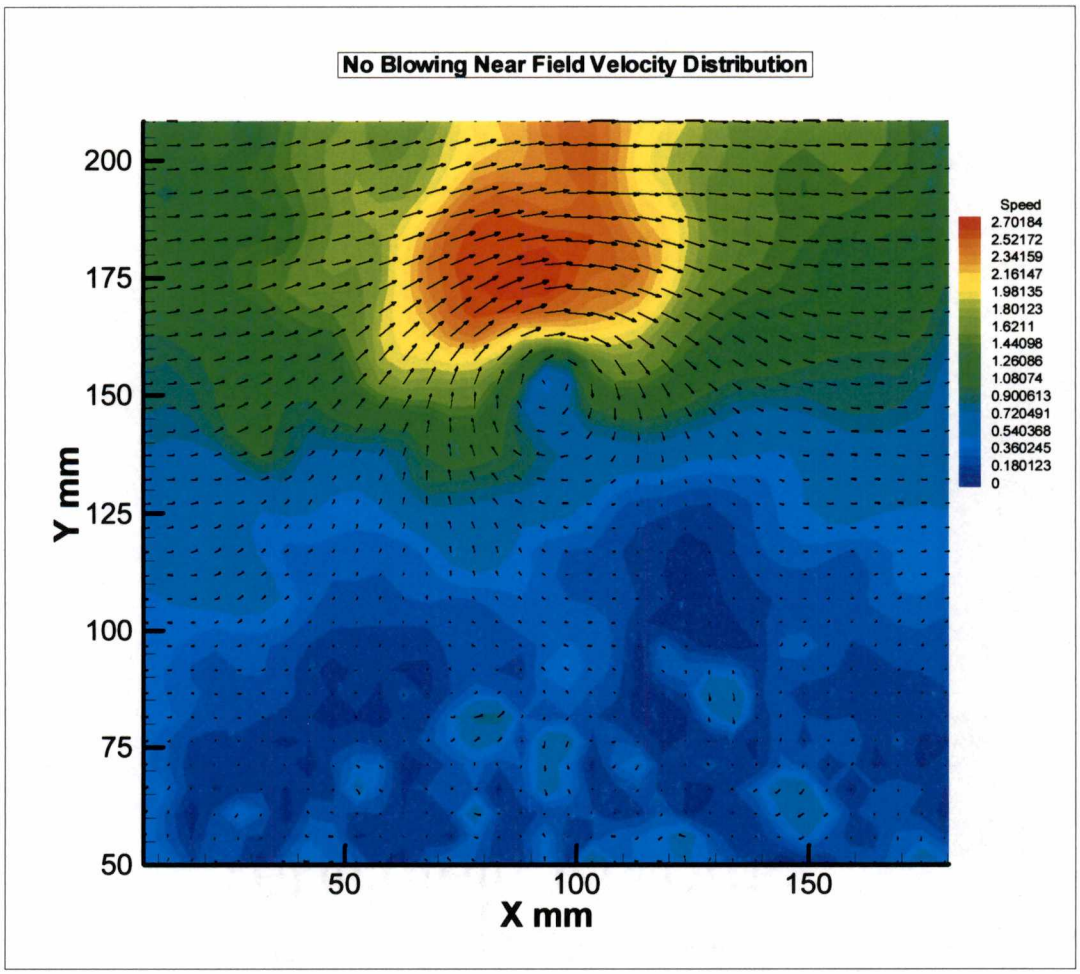


Figure 4-8. PIV Results – No Blowing, Near Field Velocity Contour
(RPM = 240, Re = 0.3 X 10^6)

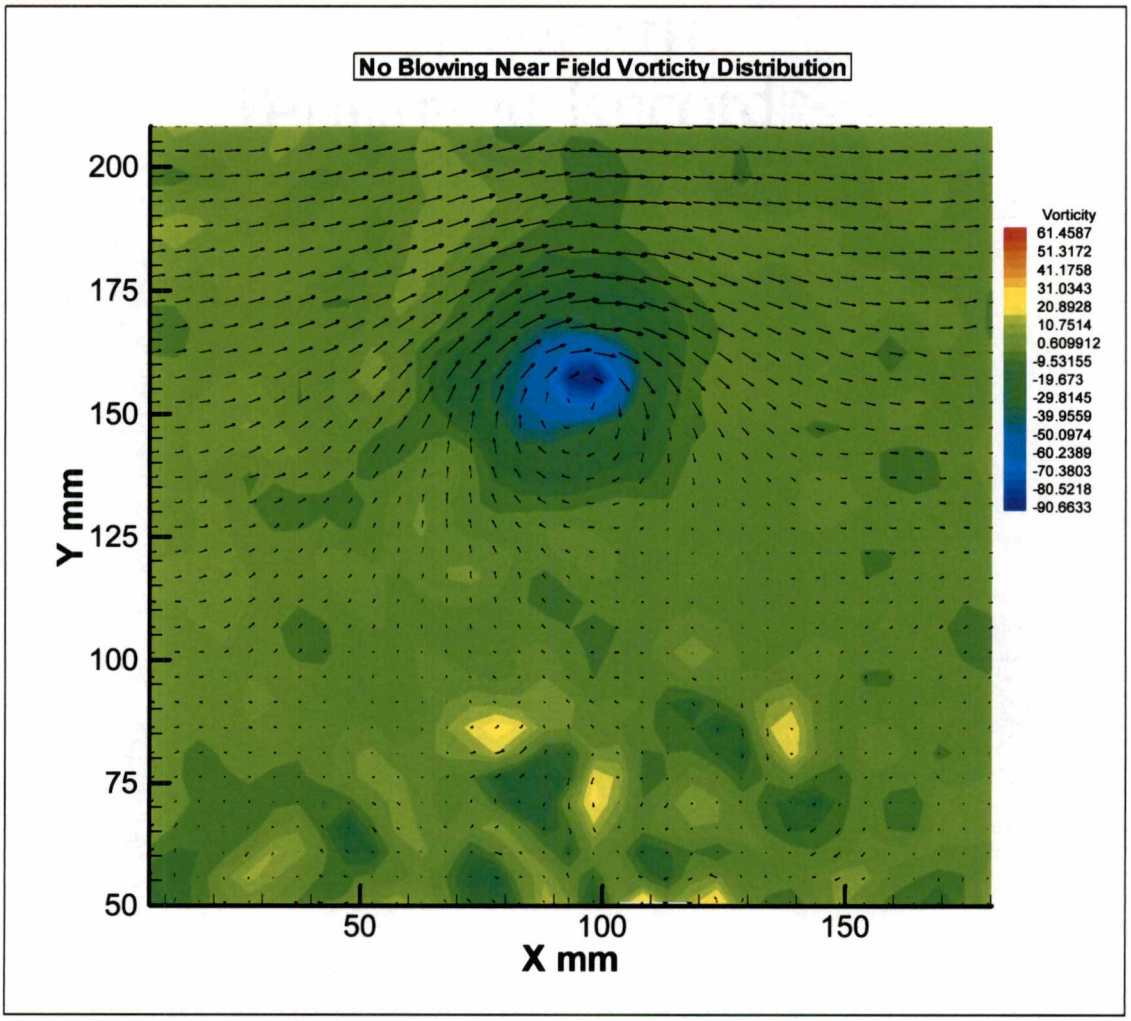


Figure 4-9. PIV Results – No Blowing, Near Field Vorticity Contour
(RPM = 240, Re = 0.3 X 10^6)

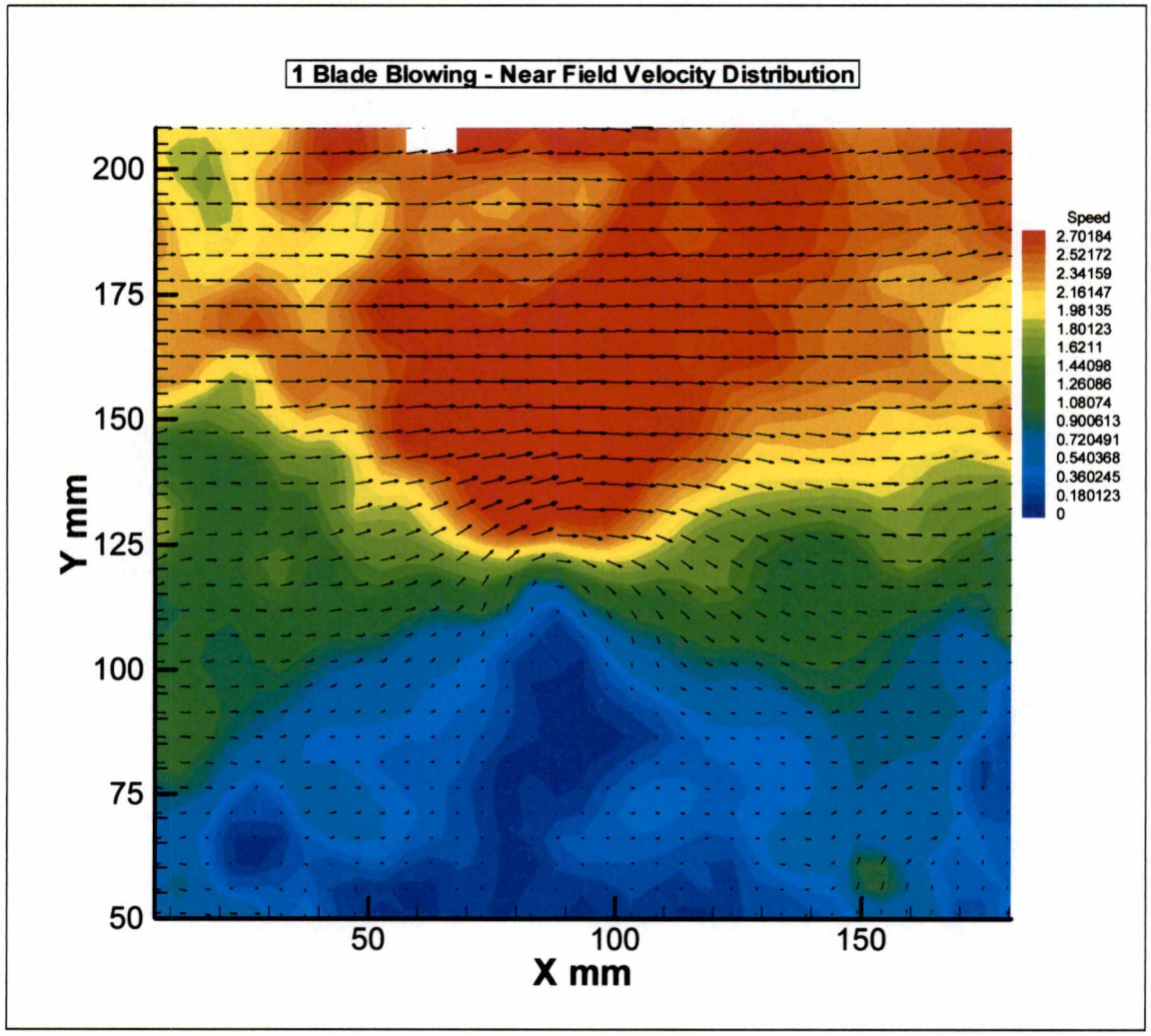


Figure 4-10. PIV Results – 1 Blade Blowing, Near Field Velocity Contour (RPM = 240, Re = 0.3 X 10^6, Cμ=0.0255)

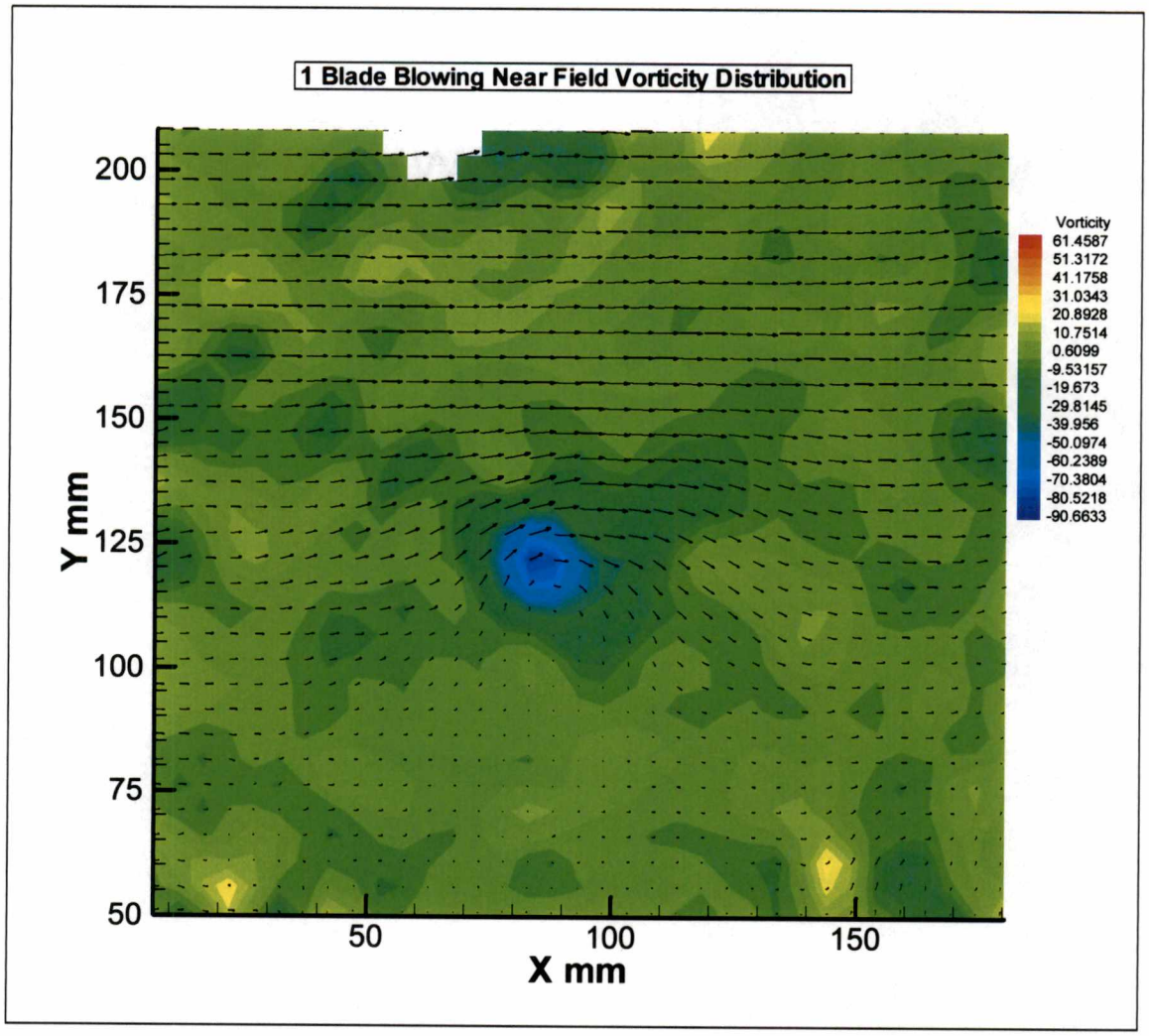


Figure 4-11. PIV Results – 1 Blade Blowing, Near Field Vorticity Contour
(RPM = 240, Re = 0.3 X 10^6, Cμ=0.0255)

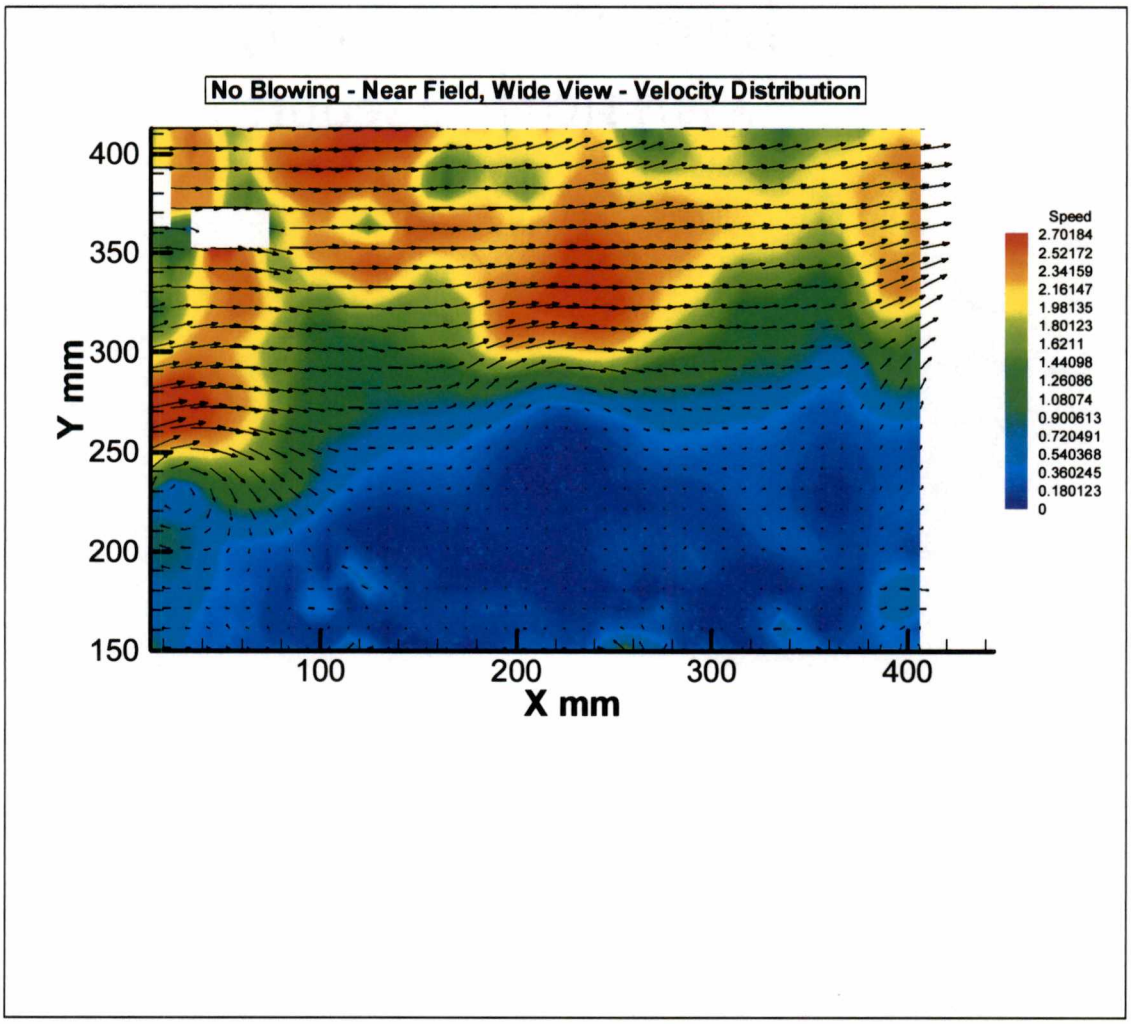


Figure 4-12. PIV Results – No Blowing, Near Field, Wide View Velocity Contour (RPM = 240, Re = 0.3 X 10^6)

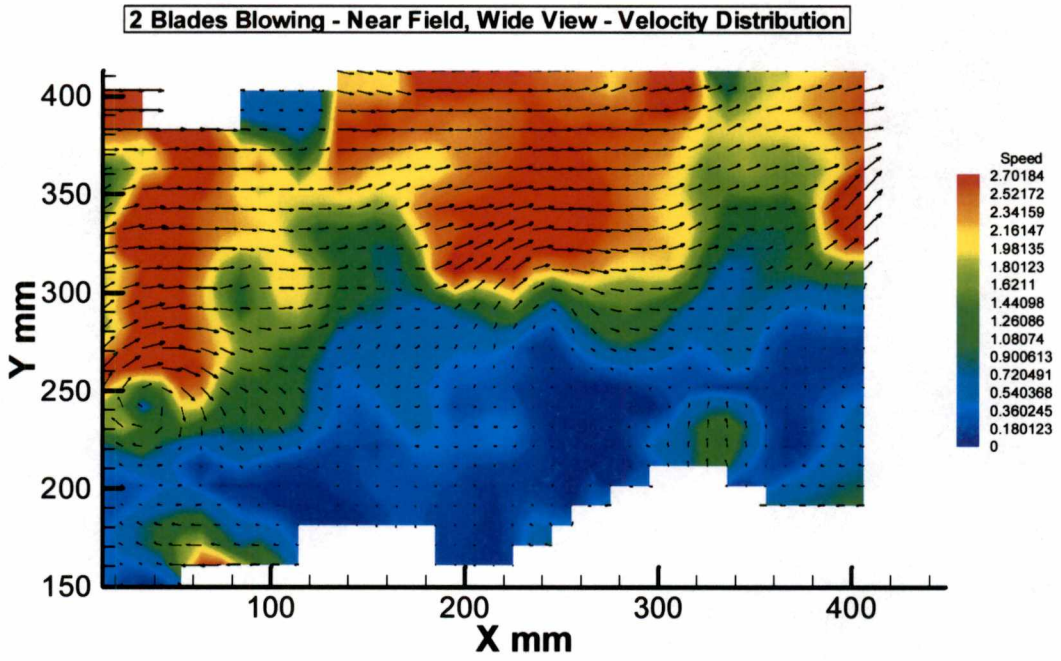


Figure 4-13. PIV Results – 2 Blades Blowing, Near Field, Wide View
Velocity Contour
(RPM = 240, Re = 0.3 X 10^6, Cμ=0.020)

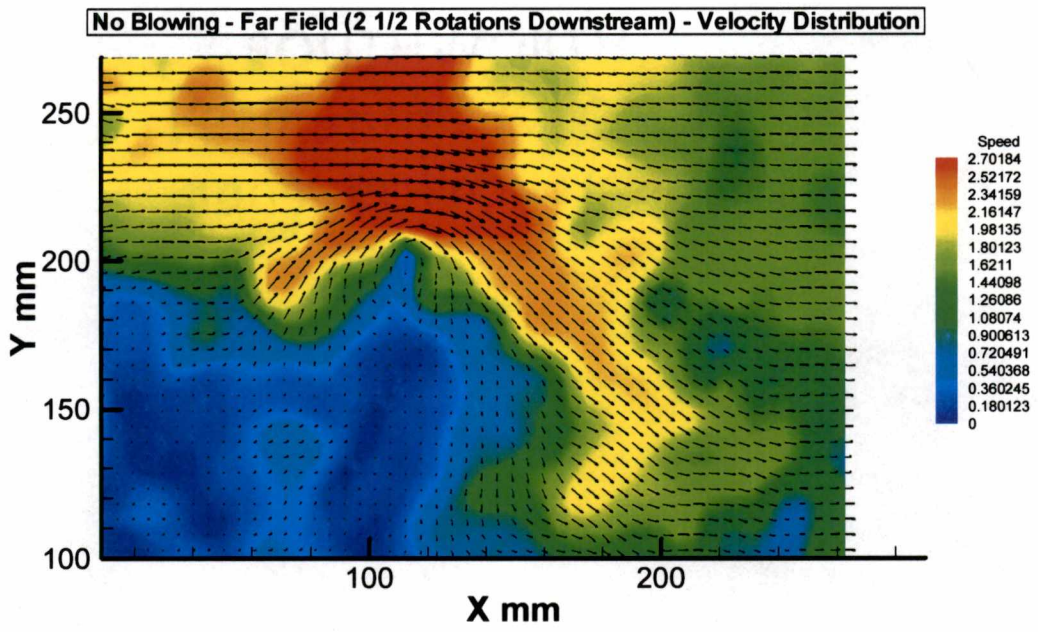


Figure 4-14. PIV Results – No Blowing, Far Field Velocity Contour
(RPM = 240, Re = 0.3 X 10^6)

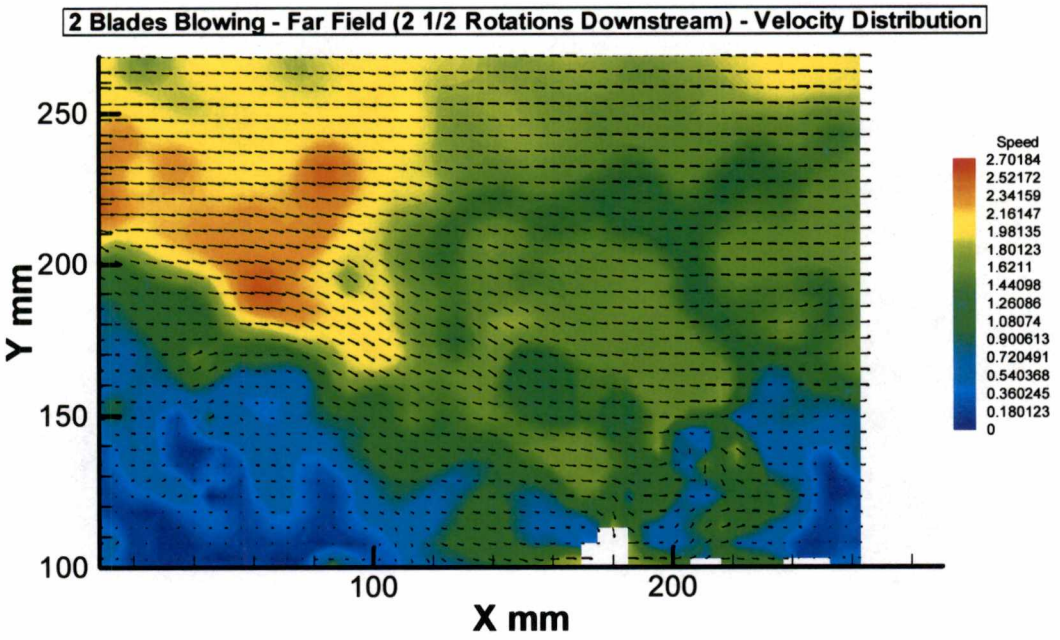


Figure 4-15. PIV Results – 2 Blades Blowing, Far Field Velocity Contour
(RPM = 240, Re = 0.3 X 10^6, Cμ=0.020)

Limitations of the Study

As with most unfunded experimental investigations, there were several limitations imposed on this study. The most significant problem encountered was related to the deficiencies in seeding the flow field. Although atomized oil particles proved adequate (marginally) for most of the areas of interest in this investigation, more complete data, which would require less post-processing, could have been collected if better seed particles and better seeding methods were available. The atomized water approach to seeding the flow field demonstrated great potential, however air pressures greater than that available in the lab would be required to properly utilize water particles in the seeding activity. If further PIV investigations are conducted on the rotor test stand, atomized water as a seeding particle technology should be developed.

As mentioned in the discussion of the observed data, it was noted that vortex meandering occurred during many test series (especially during blowing configurations). Although rotor vortex meandering is a know phenomenon[3,8,9,22] there also exists the possibility that recirculation of the air in the test area could have contributed to this occurrence. Further, as was observed, very small differences in rotor blade angle of attack resulted in the merging of shed vortices. This effect was minimized to the maximum extent possible, however it could not be eliminated entirely and could have contributed to vortex wandering. It should be noted that by minimizing the difference between the blade angles of attack, the frequent differences between maximum velocities observed by Matthewson[23] between the two blades for the same (baseline) configuration were likely reduced greatly.

In as much as Matthewson's results[23] were limited by the fact that he could only measure effective velocities, the PIV measurements presented here were limited by their planar nature. Obviously, a rotor flow field is highly three dimensional and as a result many PIV data images presented here exhibit small indications of non-uniformity and

apparent anomalous data. This consideration was not a significant limitation, so long as its effects were considered when viewing data.

CHAPTER V

CONCLUSIONS AND RECOMMENDATIONS

An experimental study of the effects of vortex flow control on a model rotor blade using perturbations introduced by discrete tip jets has been conducted. Smoke flow visualization was conducted to qualitatively investigate the physics of the flow field. As well, PIV measurements at several positions and with differing fields of view were carried out to quantify the effects of blowing on the velocity and vorticity distribution associated with rotor blade tip vortices.

Visualization of the vortices shed from the modified blade (with blowing at $C\mu$ = 0.0774) revealed a slightly altered path of travel as compared to the baseline case. This change in trajectory could be related to the interaction of the blowing and non-blowing vortices shed within the same rotor flow field. Similar interactions which resulted in vortex merging were observed when minor differences in rotor blade angle of attack existed. Flow visualization also indicated decreased vortex coherence and strength occurred as a result of discrete jet usage.

PIV measurements in the near field indicated that the use of discrete jets ($C\mu \cong$ 0.02) caused significant redistribution of vorticity and energy (i.e. dispersed velocity) away for the vortex. The dispersion of vorticity and the decrease in velocity gradients suggested that much lower impulsive noise would be generated in the event of a vortex-blade interaction. Far field measurements located 2 ½ rotations downstream indicated that discrete jets effectively dispersed the tip vortex as compared to the baseline case.

Both the qualitative and quantitative results suggested that discrete jet blowing at the rotor blade tip would be effective at minimizing the impulsive noise and vibration experienced in a blade-vortex interaction. Further, the rapid dispersion of the vortex in

the far field suggested discrete jet technology could have many useful applications in the area of accelerated fixed wing vortex dispersion.

Notwithstanding these conclusions, further investigation is required before the complete capabilities of discrete jets are understood for both the fixed wing and the rotary wing cases. In particular, additional far field investigations should be conducted to substantiate those observations made during the conduct of this investigation. Improved flow seeding is critical for this to be conducted. In addition, improved blade angle matching should be investigated, to ensure that the "merging" effect is negligible. Future tests should also address the optimization of blowing for the rotor application. Previous studies[8,18,19,20,21] have indicated that the amount of blowing could be optimized for the flow conditions that exist. Such an optimization would reveal the true potential effectiveness of discrete jets.

LIST OF REFERENCES

LIST OF REFERENCES

1. Pullin, D.I. and Saffman, P.G., "Vortex Dynamics in Turbulence", Annual Review of Fluid Mechanics, 1998, pages 31 to 51.
2. Karamcheti, K., "Principles of Ideal-Fluid Aerodynamics" Krieger Publishing Co., 1980.
3. Green, S.I., "Fluid Vortices" Kluwer Academic Publishers, 1995.
4. Fradenburgh, E.A., "Basic Aerodynamics for Rotor Performance", AGARD Report No. 781 Aerodynamics of Rotorcraft.
5. Leishman, J. and Bagai, A., "Challenges in Understanding the Vortex Dynamics of Helicopter Rotor Wakes", 27th AIAA Fluid Dynamics Conference, AIAA Paper No. 96-1957, New Orleans, LA, June 1996.
6. Rockwell, D., "Vortex-Body Interactions", Annual Review of Fluid Mechanics, 1998, pages 199 to 229
7. Sarpkaya, T., "Vortex Breakdown & Turbulence", 33rd Aerospace Sciences Meeting and Exhibits, AIAA Paper No. 95-0433, Reno, NV, January 1995.
8. Gilliam, F.T., "An Investigation of the Effects of Discrete Wing Tip Jets on Wake Vortex Roll-Up", Ph.D. Dissertation, University of Tennessee, Knoxville, August 1983.
9. Jacob, J.D., "Experimental Investigation of the Trailing Vortex Wave of Rectangular Airfoils", Ph.D. Dissertation, University of California at Berkeley, December 1995.
10. Crow, S.C., "Stability Theory for a Pair of Trailing Vortices", AIAA Journal, Vol. 8, December 1970, pp. 2172-2179.
11. Reid, E.G., "The Effects of Shielding the Tips of Airfoils", NACA Report No. 201, 1925.
12. Whitcomb, R.T., "A Design Approach and Selected Wind Tunnel Results at High Subsonic Speeds for Wing Tip Mounted Winglets", NASA TN D-8260, July 1976.

13. Mullins, B.R., Smith, D.E., Rath, C.B., and Thomas, S.L., "Helicopter Rotor Tip Shapes for Reduced Blade Vortex Interaction – An Experimental Investigation Part II", 34th Aerospace Sciences Meeting and Exhibits, AIAA Paper No. 96-0149, Reno, NV. January 1996.

14. Lee, C.S., Tavella, D., Wood, N.J., and Roberts, L., "Flow Structure and Scaling Laws in Lateral Wing Tip Blowing", AIAA Journal, Vol. 27, No.8, Paper No. 86-1810, 1988.

15. Lee, C.S., Tavella, D., Wood, N.J., and Roberts, L., "Lift Modulation with Lateral Wing-Tip Blowing", Journal of Aircraft, Vol. 25, No. 4, April 1988.

16. Lee, C.S., Tavella, D., Wood, N.J., and Roberts, L., "Influence of Wing-Tip Configuration on Lateral Blowing Efficiency", AIAA 24th Aerospace Sciences Meeting.

17. Rennich, S.C. and Lele, S.K., "A Method for Accelerating the Destruction of Aircraft Wake Vortices", AIAA 36th Aerospace Sciences Meeting and Exhibit, AIAA 98-0667, Reno, NV, January, 1998.

18. Wu, J.M., Vakili, A.D. and Chen, Z.L., "Wing Tip Jets Aerodynamic Performance", Proceedings of the 13th Congress of the International Council of the Aeronautical Sciences, ICAS 82-5.6.3, Seattle, WA, August, 1982.

19. Wu, J.M., Vakili, A.D. and Gilliam, F.T., "Aerodynamic Interactions of Wingtip Flow with Discrete Wingtip Jets", AIAA 2nd Applied Aerodynamics Conference, AIAA Paper No. 84-2206, Seattle Washington, August 1984.

20. Wu, J.M., Vakili, A.D., and Mo, J.D., "Investigation of Phenomena of Discrete Wingtip Jets", UTSI Report 88-06.

21. Wu, J.M., Vakili, A.D., Chen, Z.L. and Gilliam, F.T., "Investigation of the Effects of Discrete Wingtip Jets", AIAA 21st Aerospace Sciences Meeting, AIAA Paper No. 83-0546, Reno, NV, January 1983.

22. McAlister, K.W., "Measurements in the Near Wake of a Hovering Rotor", 27th AIAA Fluid Dynamics Conference, AIAA Paper No. 96-1958, New Orleans, LA, June 1996.

23. Matthewson, C.S., "Experimental Study of Effects of Discrete Jets on Tip Vortex Attenuation" Masters Thesis, The University of Tennessee Space Institute, August 1996.

24. TSI "Particle Image Velocimetry (PIV): Theory of Operation", Part Number 1990755A, Revision A dated September, 1995.

25. TSI "Model 610032 LaserPulse Synchronizer Instruction Manual", Part Number 1990851, dated April, 1997.

26. Melling, A. and Whitelaw, J.H., "Seeding of Gas Flows for Laser Anemometry", DISA Information dated January, 1973.

27. Adrian, R.J., "Strategies for Imaging Flow Fields with PIV", 27th AIAA Fluid Dynamics Conference, AIAA Paper No. 96-1988, New Orleans, LA, June 1996.

28. TSI "EditVec PIV Vector Editing and Post Processing & Tecplot PIV Quick Macro Panel Operation Manual", Version Beta 0.5 dated September 19, 1997.

VITA

Derek Keith Gowanlock was born on 26 January 1971 in Camrose, Alberta Canada. After attending public school in his hometown of Forestburg, Alberta he graduated from Forestburg Senior High School in June 1988 and immediately joined the Canadian Armed Forces. After completing basic training, Officer Cadet Gowanlock attended Royal Roads Military College in Victoria, British Columbia and the Royal Military College of Canada in Kingston, Ontario, graduating in May 1992 with a Bachelor's Degree in Mechanical Engineering. After completion of occupational training as an Aerospace Engineering Officer, 2nd Lieutenant Gowanlock was posted to 435 Transport Squadron in Edmonton, Alberta as a maintenance officer for the squadron's fleet of 13 CC-130 Hercules aircraft. While in Edmonton, Lieutenant Gowanlock also occupied the positions of Wing Armament Officer and was the Explosive Ordnance Disposal Centre Chief. In August 1994, Lieutenant Gowanlock was posted to the Aerospace Engineering Test Establishment in Cold Lake, Alberta where he was employed in the Fighter Evaluation Section as an Armament Test Engineer. Captain Gowanlock was subsequently selected by the Canadian Armed Forces for postgraduate training at the University of Tennessee Space Institute where he completed a Masters of Science degree in Aerospace Engineering in August 1998.